Journal of Controlled Release 386 (2025) 114038

Contents lists available at ScienceDirect

Journal of Controlled Release

journal homepage: www.elsevier.com/locate/jconrel

Advanced peptide nanoparticles enable robust and efficient delivery of gene editors across cell types

Oskar Gustafsson [a,b,*], Supriya Krishna [c,d], Sophia Borate [e], Marziyeh Ghaeidamini [f], Xiuming Liang [a,b], Osama Saher [a,b,g,h], Raul Cuellar [a,b], Björn K. Birdsong [i], Samantha Roudi [a,b,g], H. Yesid Estupiñán [a,b,j], Evren Alici [e], C.I. Edvard Smith [a,b], Elin K. Esbjörner [f], Simone Spuler [c,d], Olivier Gerrit de Jong [k], Helena Escobar [c,1], Joel Z. Nordin [a,b,l,*,1], Samir E.L. Andaloussi [a,b,g,*,1]

[a] Department of Laboratory Medicine, Unit for Biomolecular and Cellular Medicine, Karolinska Institutet, Stockholm, Sweden
[b] Karolinska ATMP center, Karolinska Institutet, Karolinska University Hospital, SE-17176 Stockholm, Sweden
[c] Muscle Research Unit, Experimental and Clinical Research Center (ECRC), a joint cooperation between the Charité – Universitätsmedizin Berlin and the Max Delbrück Center for Molecular Medicine in the Helmholtz Association (MDC), 13125 Berlin, Germany
[d] Department of Biology, Chemistry, and Pharmacy, Freie Universität Berlin, 14195 Berlin, Germany
[e] Department of Medicine, Center for Hematology and Regenerative Medicine, Karolinska Institutet, Huddinge, Stockholm, Sweden
[f] Division of Chemical Biology, Department of Life Sciences, Chalmers University of Technology, Kemivägen 10, 412 96 Gothenburg, Sweden
[g] Department of Cellular Therapy and Allogeneic Stem Cell Transplantation (CAST), Karolinska University Hospital, Huddinge, Sweden
[h] Department of Pharmaceutics and Industrial Pharmacy, Faculty of Pharmacy, Cairo University, 11562 Cairo, Egypt
[i] Department of Fibre and Polymer Technology, KTH Royal Institute of Technology, Teknikringen 58, Stockholm, Sweden
[j] Departamento de Ciencias Básicas, Universidad Industrial de Santander, Bucaramanga, Colombia
[k] Department of Pharmaceutics, Utrecht Institute for Pharmaceutical Sciences (UIPS), Utrecht University, Universiteitsweg 99, 3584 CG, Utrecht, the Netherlands
[l] Department of Clinical Immunology and Transfusion Medicine (KITM), Karolinska University Hospital, 141 86 Stockholm, Sweden

ARTICLE INFO

Keywords:
Synthetic gene editor delivery
Protein delivery
Cell-penetrating peptide (CPP)
Diverse cells, including MuSC and iPSC
Gene editing
Base and primer editor

ABSTRACT

Efficient delivery of the CRISPR/Cas9 system and its larger derivatives, base editors, and prime editors remain a major challenge, particularly in tissue-specific stem cells and induced pluripotent stem cells (iPSCs). This study optimized a novel family of cell-penetrating peptides, hPep, to deliver gene-editing ribonucleoproteins. The hPep-based nanoparticles enable highly efficient and biocompatible delivery of Cre recombinase, Cas9, base-, and prime editors. Using base editors, robust and nearly complete genome editing was achieved in the human cells: HEK293T (96%), iPSCs (74%), and muscle stem cells (80%). This strategy opens promising avenues for ex vivo and, potentially, in vivo applications. Incorporating silica particles enhanced the system's versatility, facilitating cargo-agnostic delivery. Notably, the nanoparticles can be synthesized quickly on a benchtop and stored as lyophilized powder without compromising functionality. This represents an important advancement in the feasibility and scalability of gene-editing delivery technologies.

1. Introduction

CRISPR/Cas9 and its derivatives, such as base editors (BEs) and prime editors (PEs), have emerged as the most powerful tools for genome editing. Compared to earlier technologies like Transcription activator-like effector nuclease and zinc finger nucleases, CRISPR offers simple targeting and modification of cellular DNA. [1,2]. However, the relatively large Cas9 protein and guide RNA (gRNA) present challenges for intracellular delivery, particularly when using adeno-associated viruses (AAVs) as delivery vectors. With their limited packaging capacity, AAVs often require the Cas9 coding sequence to be split into two vectors, complicating the delivery process. Additionally, viral delivery can result in prolonged Cas9 expression, raising concerns about on- and off-target genotoxicity [3–7].

* Corresponding authors at: Department of Laboratory Medicine, Unit for Biomolecular and Cellular Medicine, Karolinska Institutet, Stockholm, Sweden.
E-mail addresses: Oskar.Gustafsson@ki.se (O. Gustafsson), Joel.Nordin@ki.se (J.Z. Nordin), Samir.EL-Andaloussi@ki.se (S.E.L. Andaloussi).
[1] Shared last authors.

https://doi.org/10.1016/j.jconrel.2025.114038
Received 25 March 2025; Received in revised form 17 June 2025; Accepted 10 July 2025
Available online 18 July 2025

Non-viral delivery methods, particularly lipid nanoparticle (LNP)-mediated Cas9 mRNA and gRNA delivery, have gained traction as an alternative. While LNPs offer promising solutions, delivering the gene-modifying enzyme as mRNA necessitates translation within the cell, and hence, such approaches heavily rely on maximizing gRNA stability to avoid its degradation during Cas9 synthesis. Moreover, mRNA delivery often leads to high levels of protein expression, potentially increasing off-target activity and immunogenicity [8–11]. These drawbacks notwithstanding, LNPs have come to dominate the synthetic nanoparticle delivery field in basically every possible metric. However, achieving efficient and specific delivery to extrahepatic tissues remains a challenge [12,13]. Additionally, clinical use of LNPs is occasionally associated with adverse effects, including immunogenicity, often attributed to the presence of polyethylene glycol (PEG) [14–16]. LNP research requires significant resources, limiting the research to large labs, industry or industry collaborations. Lastly, overreliance on LNPs raises concerns about potential scientific stagnation if the technology reaches a developmental plateau. To mitigate this risk, it is essential to diversify research efforts across alternative delivery platforms, fostering innovation and ensuring continued progress.

Cas9-gRNA ribonucleoprotein (RNP) complex delivery confers substantial advantages in gene editing due to its transient bioavailability, which minimizes off-target effects, eliminates the risk of genomic integration, and mitigates immune responses against the bacterially derived Cas9 protein [17,18]. Despite these benefits, delivering Cas9 and its derivatives as RNP poses unique challenges. Unlike nucleic acids, Cas9 RNP lacks consistent charge and hydrophobicity, making it sensitive to denaturing buffers and complicating its effective delivery [19].

Thus, there is a pressing need for alternative methods to achieve efficient intracellular delivery of Cas9 RNP and its derivatives. Current strategies fall into two broad categories: physical and nanoparticle-based approaches. Physical methods, including microinjection, electroporation, and membrane deformation techniques, are highly effective but face limitations such as specialized equipment, difficulty in scaling, and limited applicability for in vivo applications [20–24].

Another strategy for RNP delivery involves the use of biological nanoparticles such as virus-like particles (VLPs) and extracellular vesicles (EVs) [25,26]. These systems are efficient and often have shown beneficial low toxicity profiles upon administration via different routes. While achieving high levels of editing in vitro and in vivo [26,27]. However, their production remains labor-intensive at the required scale, and the use of viral proteins, for delivery and endosomal escape, raises concerns regarding biological compatibility and potential immunogenicity. Furthermore, these particles often exhibit poor systemic distribution, with a tendency to accumulate in the liver [28]. The synthetic nanoparticle-based approaches have made substantial gains in recent years, achieving high editing efficiencies both in vitro and in vivo [11,29,30]. However, closer inspection of these and most other self-assembling nanoparticle publications reveals a clear tendency to use serum-free conditions, indicating particle instability in serum, which would be highly detrimental for most in vivo applications.

A promising alternative involves the use of cell-penetrating peptides (CPPs). These peptides can either be covalently attached to Cas9 or mixed to form nanoparticles with the Cas9 RNP, mainly by charge-based electrostatic interactions. While direct conjugation of CPPs with Cas9 creates a self-deliverable complex, this approach often requires large quantities of RNP due to inefficient intracellular delivery [31–35]. Furthermore, direct conjugation to the cationic CPP risks diminishing the function of the RNP while not protecting from serum proteases and RNAses [32,36]. The non-covalent strategy typically relies on charge interactions between the RNP and CPPs, leading to nanoparticle formation. This approach has proven efficient for cellular transfection and delivering various cargo types, such as RNPs and homology-directed repair (HDR) templates [37]. Previously established cell-penetrating peptides, such as TAT, Transportan, and Penetratin, have been shown to be ineffective for Cas9 RNP delivery—both when covalently linked to the RNP and when used as co-administered assist peptides—as demonstrated by Zhang et al. [38]. In addition, CPPs commonly suffer from poor serum stability, with multiple studies reporting a significant reduction in their effectiveness in the presence of serum, particularly for peptides like TAT [39–42]. Notably, CPP-based Cas9 RNP delivery methods such as PERC and PAGE, both rely on simple co-incubation strategies, typically require low or serum-free conditions to achieve efficient delivery. [33,38]. This underscores the critical need for scalable, serum-compatible delivery methods for Cas9 and its larger derivatives. Such systems are essential for gene editing in cells and tissues, including iPSCs and skeletal muscle, where non-viral delivery remains a major hurdle. iPSCs offer vast therapeutic and research potential, while more than 40 different monogenic disorders affect skeletal muscle, leading to progressive degeneration and atrophy—conditions for which effective treatments are still lacking [43]. Skeletal muscle contains a tissue-specific population of muscle stem cells (MuSCs) that play a critical role in muscle regeneration, making them ideal candidates for cell replacement therapies [44]. In the case of autologous applications within muscular dystrophy, the disease-causing genetic defect needs to be repaired before transplanting the cells back into the patient. Efficient and safe non-viral ex vivo delivery of genome editing tools is an essential first step toward achieving this goal.

In this study, we characterized and adapted a family of CPPs known as hPep, previously used to deliver nucleic acids, for efficient RNP-based delivery of Cas9 and its derivatives [45]. During particle formation, enhanced delivery was achieved by incorporating silica as a core to the nanoparticle. This allowed for highly efficient delivery across cell types at low doses and the delivery of more challenging cargos, such as prime editor and corresponding pegRNAs. hPep nanoparticles demonstrated virtually unaltered activity in serum conditions, irrespective of protein cargo. Furthermore, hPep enabled base editor delivery to primary cells such as MuSCs and iPSCs while preserving myogenic and pluripotency markers, respectively. The ability of hPep to efficiently deliver diverse cargos across various cell types represents a major advancement toward a simple synthetic system. This system can be easily prepared in minutes on a benchtop, stored as lyophilized powder, and applied using standard laboratory techniques.

2. Results

2.1. hPep-mediated delivery of Cas9-RNPs in reporter cells shows efficient delivery in full serum after formulation optimization

Cationic CPPs, initially designed for nucleic acid delivery, have been shown to form particles with Cas9 RNPs, facilitating intracellular delivery [46]. To adapt the hPep family of CPPs for RNP delivery, four peptides were selected with identical amino acid sequences but varying alkenyl-alanine moieties, all with a total net charge of +6 (Table 1, Supplementary Fig. 1A). These peptides are amphipathic, with a strong cationic charge on one side and hydrophobic moieties on the other, as can be seen in the helical projection of the peptide (Fig. 1A) [47]. The peptides were screened for their ability to deliver Cas9 RNP by combining the two components at different molar ratios (MR), RNP to CPP, followed by the addition to HEK293T Stop light (SL) reporter cells, which express GFP upon successful editing by Cas9 (Fig. 1A) [48]. The GFP expression of the SL system has previously been validated to align with the underlying genetic edit [37,46]. Among the candidates, hPep3 and hPep4 exhibited the highest delivery efficiency (Fig. 1B), whereas treatment with naked RNP resulted in editing below the assay's detection limit, as shown by others [37].

Next, various methods were used to characterize the formed nanoparticles, such as an electrophoretic mobility shift assay (EMSA), which confirmed nanoparticle formation at a low MR of 1:25 (Fig. 1B). However, optimal functional delivery was achieved at MRs 1:200 and above (Fig. 1B). A hexametaphosphate stability test revealed that hPep4-formed particles were slightly more stable than those formed by

Table 1
gRNAs, oligos, and peptide sequences.

gRNAs	Target Sequence
Stop light (Cas9)	GGACAGTACTCCGCTCGAGT
Stop light 3 (HDR)	CTTACTTGTACAGCTCGTCC
Stop light 3 (Prime)	AAGCTCTTCACCCTTAGACA
Base editor Yachie (ABE8e)	CCTTATGACCCTGACACGCT
B2M (ABE8e)	ACTCACGCTGGATAGCCTCC
NCAM1 (ABE8e)	CCCTACCAAAGACTTTGAGG
Oligos	**Sequence**
PCV-oligo	AAGTATTACCAGAAAACAGCAATTTCAGCGATTTAACCAGTACAACGAACACGTCTACCT
61 bp SL3 (+)	TCTACGGGCGGCCTGGACGAGCTGTACAAGCAAGCCGTGTCTAAGGGTGAAGAGCTTTTCA
61 bp SL3 (−)	TGAAAAGCTCTTCACCCTTAGACACGGCTTGCTTGTACAGCTCGTCCAGGCCGCCCGTAGA
81 bp SL3 (−)	ACGACGCCCGTGAAAAGCTCTTCACCCTTAGACACGGCTTGCTTGTACAGCTCGTCCAAGCCGCCCGTAGAATGCCTGCCT
100 bp SL3 (+)	AAAGAGCTGAAGGCAGGCATTCTACGGGCGGCCTGGACGAGCTGTACAAGCAAGCCGTGTCTAAGGGTGAAGAGCTTTTC ACGGGCGTCGTTCCCATCTT
100 bp SL3 (−)	CAAGATGGGAACGACGCCCGTGAAAAGCTCTTCACCCTTAGACACGGCTTGCTTGTACAGCTCGTCCAGGCCGCCCGTAGAA TGCCTGCCTTCAGCTCTT
Peptides	**Sequence**
hPep1	H-LAKLAKA(R8)AKLLKA(S5)AKAL-NH2
hPep2	H-LAKLAKA(R8)AKLLKA(S8)AKAL-NH2
hPep3	H-L(R8)KLAKA(R8)AKLLKA(R8)AKAL-NH2
hPep4	H-L(R8)KLAKAAAKLLKA(S8)AKAL-NH2

hPep3, correlating with their higher transfection efficiency (Supplementary Fig. 1B). When particle formation was tested in different physiological buffers, HBG and Opti-MEM were the most effective, with HBG showing more consistent results between experiments (Supplementary Fig. 1C). Notably, spinfection of particles formed in HBG led to a ~ 5-fold increase in editing efficiency (Supplementary Fig. 1D).

Nanoparticle tracking analysis (NTA) indicated a homogeneous population with a median size of 129 nm at 1:200 MR (Supplementary Fig. 1E). Particle size decreased from a median size of 192 nm at MR 1:25 to a stable range of 125–130 nm at MR 1:100 and above. Additionally, the number of particles larger than 200 nm substantially decreased with increasing MR.

The Cas9 RNP delivery efficiency achieved with the hPep family peptides was lower than our previously published RNP-CPP delivery method [37,46]. Several additives were tested to enhance delivery efficiency (Fig. 1C). Among these, PVA-PEG showed the most considerable improvement, reaching nearly 80% editing efficiency and surpassing previously published plasmid-based CRISPR/Cas9 transfection results using the same reporter system [46]. It is important to note that the SL reporter system only activates GFP upon insertions or deletions of ±1 or ± 2 base pairs, which inherently limits the maximum percentage of GFP-positive cells.

Different buffers were combined with hPep3 and PVA-PEG to optimize the delivery system during nanoparticle formation (Supplementary Fig. 2A). DMEM and Opti-MEM demonstrated the highest editing efficiencies, with DMEM being selected as the base buffer for subsequent experiments. Next, all hPep peptide variants were screened using the PVA-PEG/DMEM formulation, with as little as 10 ng (0.6 nM) Cas9 per well (Supplementary Fig. 2B). The peptides hPep1 and hPep2, which initially showed minimal to no transfection efficiency, now exhibited the highest editing efficiencies, reaching ≥75%, with hPep3 closely following.

Since hPep3 performed consistently well in both HBG and PVA-PEG buffer systems, it was selected as the lead candidate for further experiments. An EMSA assay revealed nanoparticles forming at lower MRs in the PVA-PEG buffer than in HBG, with minimal RNP smearing observed across all tested MRs (Supplementary Fig. 2C). These DMEM/PVA-PEG formulated particles displayed a smaller size than those formed in HBG, with a median size around 100 nm (Supplementary Fig. 2D). Adding hPep3 to a PVA-PEG Cas9 mixture condensed the particles from 144 nm to around 100 nm.

To assess editing efficiency in traditionally harder-to-transfect cell lines, MDA-MB-231 SL and MCF-7 SL cells were treated using RNP:hPep3 particles formulated at varying concentrations of PVA-PEG (Supplementary Fig. 2E). As anticipated, editing efficiency was lower than that observed in HEK293T SL cells; however, it remained high.

Increasing amounts of FBS were introduced to the culture media to challenge the delivery system prior to transfection with Cas9 RNP:hPep3 particles (Fig. 1D, Supplementary Fig. 2F). Editing efficiency peaked at FBS concentrations ranging from 0% to 30% and gradually declined at higher FBS levels. However, editing remained detectable at 90% FBS. Additionally, the stability of the particles was evaluated under different storage conditions. The particles maintained their delivery efficiency after exposure to freeze-thaw cycles, vacuum concentration, or lyophilization (Fig. 1E, Supplementary Fig. 2G & H). These findings are consistent with our previous study, which demonstrated that RNP-CPP particles exhibit high resistance to challenging storage conditions [46]. Thus, with the right additive, these peptides can efficiently deliver Cas9 RNP to different cell types in highly demanding conditions.

The ability of previously established CPPs to deliver Cas9 RNP under the optimized conditions identified in Fig. 1 was evaluated. Despite clear cellular uptake of the peptides (Supplementary Fig. 3A & B), little to no genome editing activity was detected, indicating ineffective RNP delivery.

2.2. hPep delivers protein cargos irrespective of charge and enables efficient co-delivery of HDR DNA templates

Traditionally, non-covalent CPP-mediated transfection relies on electrostatic interactions between cationic CPPs and anionic cargo. To investigate whether hPep particle formation is enhanced by increasing these electrostatic interactions, additional anionic charges were introduced to the cargo by coupling a single-stranded DNA (ssDNA) to the fusion protein PCV-Cas9, forming a covalent bond between these two components (Supplementary Fig. 3C) [49]. However, adding the ssDNA did not improve editing efficiency (Fig. 2A). The oligo used was a random nucleotide sequence, except for the PCV binding site, designed to avoid genomic homology DNA binding, simply acting as an anionic charge carrier.

To further investigate the relevance of cargo change, the cationic hPep was complexed with the cationic protein Cre recombinase. The peptides effectively delivered Cre to various cell types expressing a Cre-LoxP traffic light (TL) reporter system (Fig. 2B, Supplementary Fig. 3D). In some instances, nearly 100% recombination efficiency was achieved. Harder-to-transfect cell lines, such as T47D breast cancer cells and immortalized mesenchymal stem cells (MSCs), required higher MR and dosages to achieve higher editing levels, reaching up to 80%. These findings suggest that cargo charge does not impact delivery efficiency

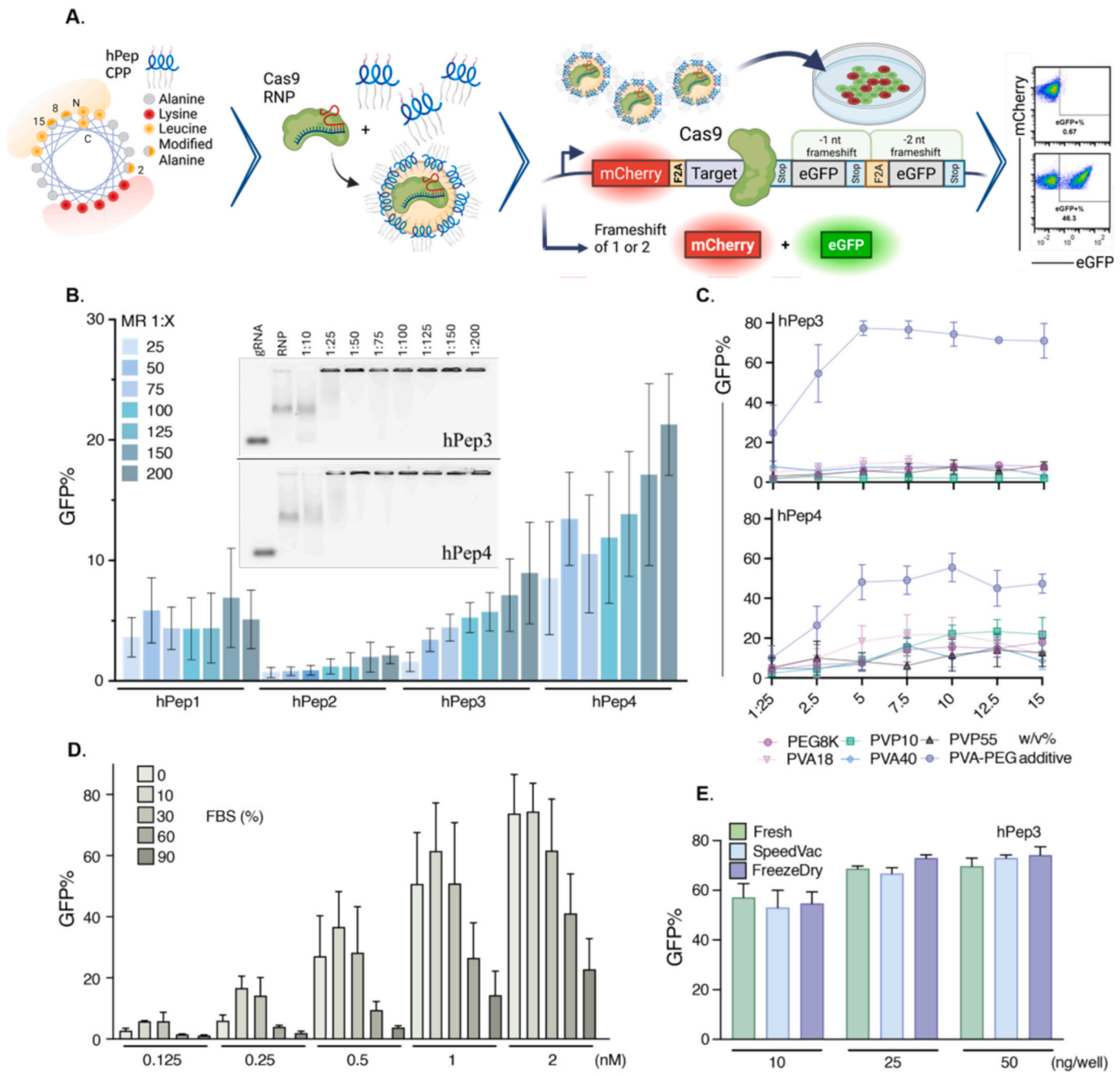

Fig. 1. Experimental design and optimization of Cas9 RNP:hPep formulations in vitro. A. Helical wheel illustration of the hPep peptide, graphical illustration of the hPep particles, a schematic showing the Stoplight reporter system, and the general analysis method. B. GFP% percentage after treatment with Cas9 RNP:hPep (200 ng Cas9 per 96-well (10.2 nM), HEK293T SL cells) with increasing MR. $n = 4$ independent experiments ± SD. Gel mobility assay to determine at what MR the RNP no longer migrates through the gel due to charge neutralization or particle size. The same gel has been spliced as shown my the horizontal line. C. Screening of additives to enhance nanoparticle efficiency using hPep3 and hPep4 (25 ng of Cas9 per 96-well (1.5 nM), HEK293T SL cells). The particles were formed in HBG diluted with the additive to a final concentration between 1.25 and 15 *w/v*%. Mean value of $n = 3$ independent experiments ± SD. D. Effect of serum on transfection efficiency of hPep3-CPP in PVA-PEG buffer (x-axis indicates conc. of Cas9 RNP added to HEK293T SL cells). One day after the transfection, serum was added to 10% in the 0% FBS condition. Mean value of n = 3 independent experiments ± SD. E. Testing of RNP:hPep3 compatibility with different storage methods (10/25/50 ng Cas9 per well (0.6, 1.5, 2,9 nM). HEK293T SL cells). Mean value of n = 3 independent experiments ± SD.

when using PVA-PEG, as strongly anionic and cationic cargo were well tolerated in hPep3-mediated delivery.

Given the minimal effect of cargo charge on delivery efficiency, an attempt was made to co-deliver a homology-directed repair (HDR) ssDNA template to SL3 reporter cells. The ssDNA was designed to enable HDR-mediated conversion of a single thymine to a cytosine, thereby converting a stop codon to a glutamine codon (Fig. 2C) [37]. Co-delivery of the HDR template resulted in ≥40% HDR rates using an 81 nt-long homologous ssDNA (Fig. 2C). Notably, the choice of strand for the ssDNA template substantially influenced the editing outcome, with substantially higher HDR rates observed when the minus strand was used (Supplementary Fig. 3E).

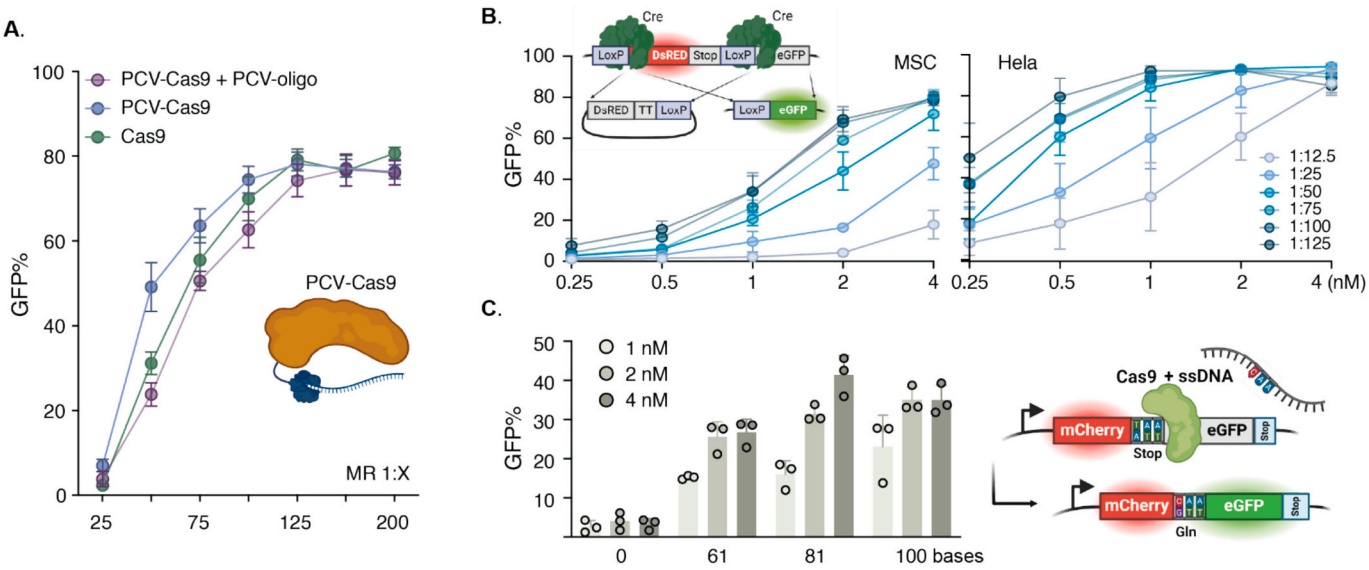

Fig. 2. Cargo-independent hPep-mediated delivery and DNA-templated HDR editing. A. Covalent attachment of a 60 nt oligo to PCV-Cas9 (53 nt after PCV binding). Particles were formed in DMEM/PVA-PEG buffer at increasing MR (15 ng protein per 96-well (0.9 nM), HEK293T cells). Mean value of $n = 3$ independent experiments ± SD. B. Cre was complexed with hPep3 in DMEM/PVA-PEG buffer at increasing MR and added to MSC and HeLa cells harboring the TL reporter system in increasing concentration of Cre. Mean value of n = 3 independent experiments ± SD. C HDR efficiency using a co-complexed ssDNA template. Particles were formed in DMEM/PVA-PEG (MR of 1:125) with increasing doses (1, 2, 4 nM) added to HEK293T harboring the SL3 system. Oligos were designed with homologous arms of equal length on each side of the expected DNA double-strand break site. Mean value of n = 3 independent experiments ± SD.

2.3. hPep-mediated delivery of gene editors does not confer cellular toxicity

Exploratory experiments pointed toward a quick mode of action, often coupled with adverse cell effects at high doses. A common solution for this is to shorten the cellular exposure time. Thus, the delivery kinetics of Cas9 RNPs using the hPep system were investigated in the SL reporter system, which requires intracellular uptake, endosomal escape, successful editing, and subsequent GFP transcription and translation for a positive signal to be detected. GFP expression was observed in treated cells as early as 4 h post-treatment, indicating rapid uptake and efficient endosomal escape (Fig. 3A). Lipofectamine RNAiMAX exhibited slower editing kinetics (Fig. 3B). RNAiMAX was used instead of CRISPRMax due to low efficiency and varied activity of CRISPRMax (Supplementary Fig. 3F).

The swift delivery of Cas9-hPep3 was further corroborated in an endosomal rupture assay using a Huh7 mCherry-GAL9 (Galectin-9) reporter cell line [50]. This reporter system relies on the recruitment of GAL9 to the site of an endosomal rupture, which can be quantified using the mCherry tag. Increasing concentrations of Cas9-hPep3 were added to the cells followed by microscopic analysis of mCherry-GAL9 puncta over 16 h (Supplementary Fig. 4A). Puncta were detectable as early as 15 min after the addition of nanoparticles, demonstrating rapid uptake and endosomal rupture with a plateau in puncta detection after 6 h (Fig. 3C). The puncta were often concentrated in the perinuclear region, suggesting cargo release in proximity to the nucleus (Fig. 3D).

Quick and extensive endosomal rupture can lead to toxicity; hence, a WST-1 assay, measuring the metabolic activity of the cells, was conducted to assess the cytotoxicity of the particles. This revealed a dose-dependent reduction in metabolic activity following treatment with either hPep or RNAiMAX (Fig. 3E, Supplementary Fig. 4B & C). Given the rapid editing observed post-treatment, an evaluation was performed to determine whether a short exposure to the particles would suffice for efficient uptake and delivery while minimizing cellular toxicity. Indeed, a 15-min incubation followed by a medium exchange yielded high editing levels while abolishing the previously observed toxicity (Fig. 3E and Supplementary Fig. 4C). A 2-h incubation resulted in equivalent editing efficiency to conditions without medium exchange but with negligible toxicity and was hence chosen for subsequent experiments. In contrast, shorter incubation times drastically reduced editing rates when RNAiMAX particles were applied (Supplementary Fig. 4D). In summary, these data show that the hPep3-mediated transfection is exceptionally rapid and that changing the media can negate adverse cellular effects.

2.4. Expanding hPep3– mediated delivery to base editors and prime editors

Recently developed Cas9 derivatives have demonstrated major therapeutic potential, enabling the treatment of previously untreatable mutations. One such derivative is the base editor ABE8e [51]. Therefore, we next wanted to assess if hPep3 is compatible with its intracellular delivery of ABEs. hPep3 and ABE8e RNP were complexed and introduced to HEK293T cells containing an integrated reporter cassette, designated HEK293T-ABE-GFP, where GFP expression is activated upon the conversion of a stop codon into a glutamine codon (Fig. 4A) [51,52]. Increasing doses of ABE8e-hPep3 particles, formulated at varying MR, were administered to HEK293T-ABE-GFP cells, resulting in editing rates of approximately 90% even at the low dose of 1 nM RNP (Fig. 4A). These high editing rates were corroborated in B16F10 and N2A cells harboring the same reporter system, demonstrating>90% editing efficiency (Supplementary Fig. 5A).

Next, ABE8e was employed to induce mis-splicing of the pre-mRNA encoding the endogenous surface protein Beta-2 Microglobulin (B2M) by mutating a splice donor site causing a protein knockout (KO), as previously reported [53]. Dose titration experiments were conducted using hPep3 and RNAiMAX to deliver the B2M-targeted ABE8e. Both modalities exhibited potent KO of B2M, with ABE8e-hPep3 achieving over 93% silencing, performing significantly better than RNAiMAX (Fig. 4B). The exact delivery method was applied to iPSCs, resulting in B2M KO rates of up to 78% and 30% in hPep3-ABE8e and RNAiMAX-treated cells, respectively (Fig. 4C). RNAiMAX was tested at lower doses due to associated cellular cytotoxicity, where the highest edited group, 4 nM ON (overnight), resulted in a 7-fold reduction in viable cells compared to the NT control. In contrast, the 6 nM ABE8e-hPep3 dose exhibited similar cell numbers and viability as the NT control three days post-treatment (Supplementary Fig. 5B). To further validate hPep as an

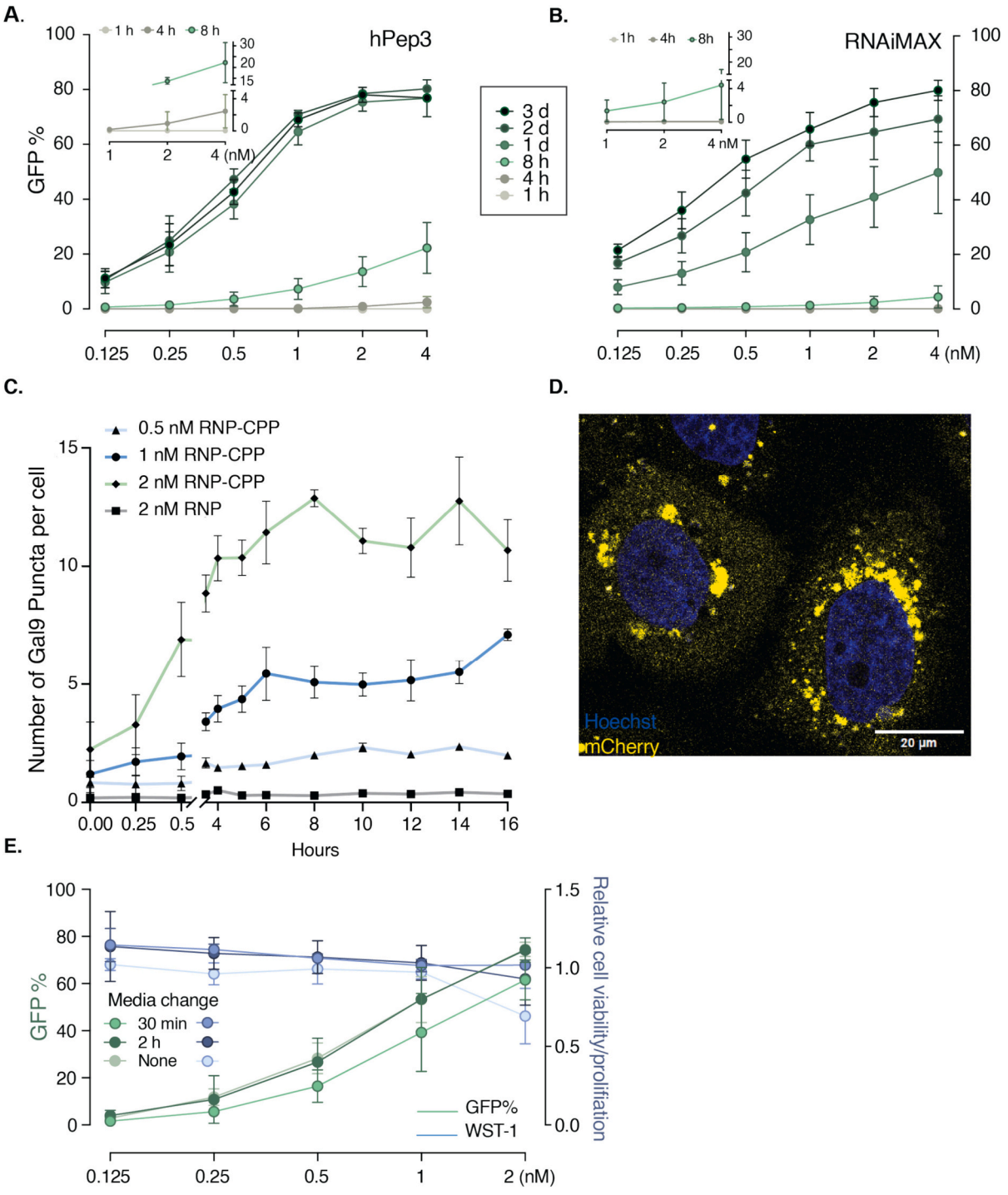

Fig. 3. Rapid uptake and endosomal escape enable robust editing without associated cellular toxicity. A. & B. Editing rates after treatment with various doses of RNP: hPep3 (1:125 MR, HEK293T) or RNP:RNAiMAX. The treatment was performed simultaneously on 6 different plates, with each plate analyzed by flow cytometry at different time points. The RNP:hPep3 treatment resulted in detectable GFP at 4 h of treatment, reaching the maximum after 24 h. Editing with RNAiMAX was first detected at 8 h, increasing each day until day 3. The short-time points are magnified in the top left corner of A & B. Mean value of $n = 3$ independent experiments ± SD. C. & D. A Huh7 mCherry-GAL9 reporter cell line was used to evaluate endosomal rupture. A rapid occurrence of rupture events after adding RNP:hPep3 formulated in DMEM/PVA-PEG was observed. n = 3 independent experiments ± SD. The rupture events were observed to cluster in the perinuclear area. E. A media change was implemented 30 min or 2 h after adding the Cas9:hPep3. Editing rates were determined based on the activation of the GFP reporter (left y-axis in green), and cytotoxicity was measured using a WST-1 assay (right y-axis in blue) of identically treated cells. A 2-h incubation resulted in editing equivalent to a 3-day incubation, while cytotoxicity was almost eliminated at all tested doses. Mean value of n = 3 independent experiments ± SD. (For interpretation of the references to colour in this figure legend, the reader is referred to the web version of this article.)

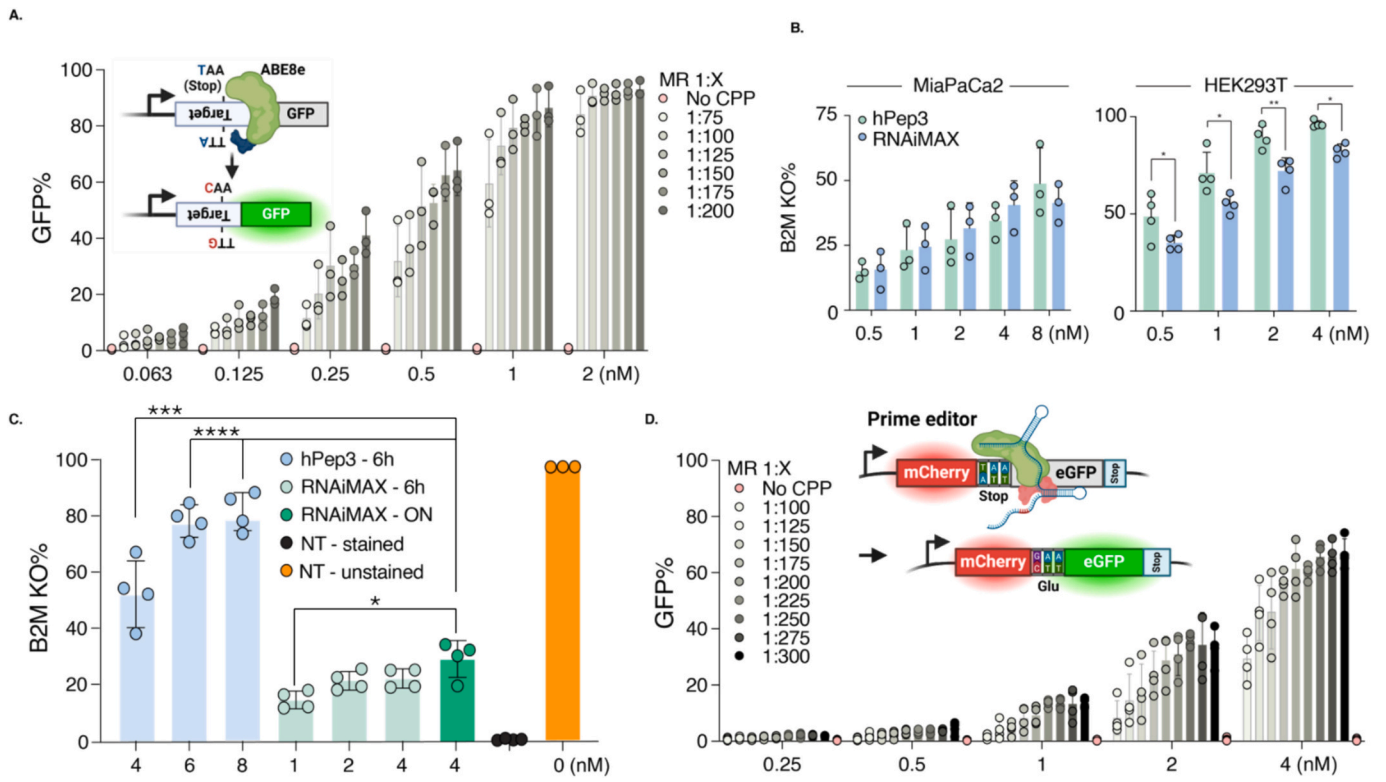

Fig. 4. hPep3-mediated ABE8e and Prime editor delivery into different cell lines and iPSCs. A. HEK293T-ABE-GFP cell was treated with an increasing dose and MR of ABE8e-hPep3 with a 2 h media change. Also shown is a schematic of the reporter construct and its mode of action. Mean value of $n = 3$ independent experiments ± SD. B. & C. ABE8e mediated Knockout of B2M in MiaPaCa2, HEK293T WT cells, and iPSC by disrupting a splice donor site using hPep3 or RNAiMAX. The cells were stained with a B2M-APC antibody and gated for negative cells 3 days after treatment. The Y-axis displays % B2M negative cells. The NT cells were 100% positive for B2M (data not shown for MiaPaCa2 and HEK293T). The hPep3 and RNAiMAX groups for MiaPaCa2 and HEK293T were analyzed using 2-way ANOVA and multiple comparisons (* indicating statistical significance of $p < 0.05$, ** < 0.01, *** < 0.001, **** < 0.0001). Mean of n = 3 (MiaPaCa2), $n = 4$ (HEK293T) independent experiments ± SD. Human iPSCs from 4 different donors were treated with independent treatments performed in triplicate. Data is shown as mean value ± SD. Editing peaked at 86.4% for the highest edited repeat. A similar trend was observed for the other lines. The ABE8e-CPP achieved significantly higher B2m KO than RNAiMAX at all tested concentrations. (* indicating statistical significance of p < 0.05, *** < 0.001, **** < 0.0001). The significance was determined using Ordinary one-way ANOVA multiple comparisons, Holm-Šídák's multiple comparisons test. D. Editing efficiencies of increasing doses and MR of PE2 given to HEK293T SL3 cells. Also shown is a schematic of the reporter construct and its mode of action. Editing reached 67%, with certain triplicates reaching 72% editing. The mean value of n = 4 independent experiments ± SD.

iPSC delivery agent, cells were treated with a high dose of ABE8e:hPep3 (10 nM) for 6 h and stained for SSEA-4 (pluripotency marker) after 3 days. The cells maintained a high expression level of the SSEA-4 marker (Supplementary Fig. 5B).

Another Cas9-derivate are prime editors, which hold tremendous therapeutic potential and enable precise gene manipulation such as removing, inserting, or modifying tens of base pairs—capabilities beyond those of Cas9 and base editors [54]. However, prime editors are among the largest Cas9 derivatives and lack efficient synthetic delivery systems. To address this, hPep3 was investigated as a delivery system for the PE2 variant. PE2 RNP complexes were formulated with hPep3 similarly to the ABE8e and delivered to SL3 HEK293T cells harboring a reporter cassette. This reporter system activates GFP expression upon successful prime editing by converting a stop codon into a glutamic acid codon, thereby inducing GFP expression (Fig. 4D). A dose-dependent increase in GFP-expressing cells in treated wells was observed, reaching up to 70% at the highest RNP dose and PE2:CPP molar ratio. The PE2 delivery was corroborated by targeting the ABE8e reporter locus, achieving robust levels of editing using two different pegRNA (Supplementary Fig. 5C). These results show an early example of prime editor RNP delivery using a synthetic RNP delivery system and unusually high editing efficiencies in iPSCs.

2.5. Colloidal silica enables protein absorption and is vital for high-efficiency RNP delivery

The fact that PVA-PEG addition in hPep formulations substantially improved editing efficiencies across all tested proteins, including the cationic Cre and large prime editors, prompted us to examine the role of the PVA-PEG additive. During the manufacturing process of PVA-PEG, colloidal anhydrous silica particles are added to aid in the spray-drying of the PVA-PEG. Silica is known for its ability to adsorb proteins, peptides, and nucleic acids and has been used in various transfection methods, although none involving CPPs [55–60]. Further investigation was warranted, given the presence of silica in the PVA-PEG and its potential role in enhancing the potency of hPep-formulated nanoparticles.

A gel electrophoresis showed that the Cas9 protein did not migrate into the gel when PVA-PEG was present (Fig. 5A). At the same time, a hexametaphosphate challenge indicated a weak interaction between the RNP and silica (Supplementary Fig. 5D). Silica was next isolated from the PVA-PEG solution by centrifugation and imaged using scanning electron microscopy, revealing particles in the sub-50 nm range (Fig. 5B). When silica-depleted PVA-PEG supernatant was used as a formulation buffer, a marked decrease in transfection efficiency was observed compared to non-depleted PVA-PEG (Fig. 5C). Energy-dispersive x-ray spectroscopy confirmed the presence of silica in the pellet and none in the supernatant (Supplementary Fig. 5E).

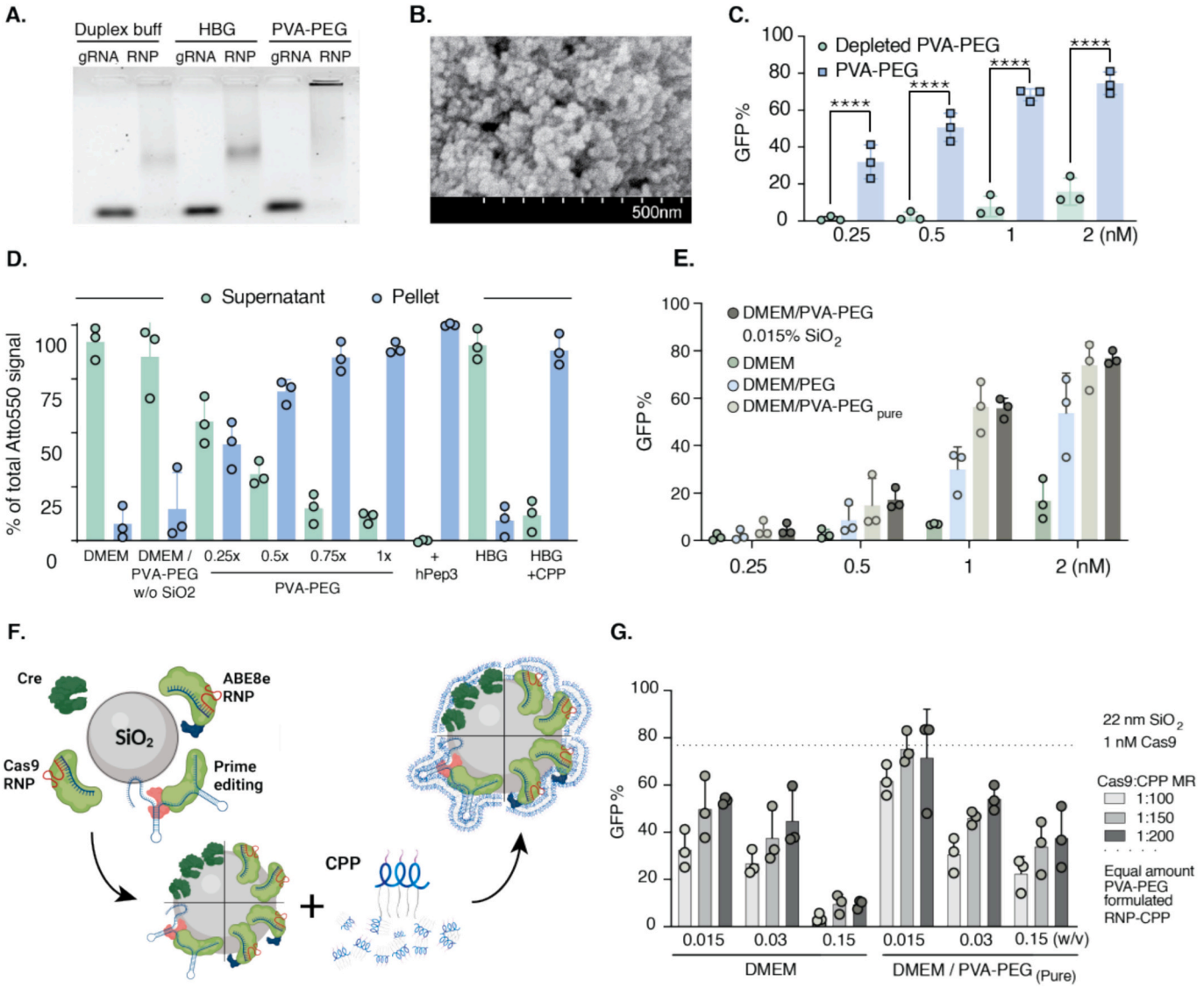

Fig. 5. Exploration of the RNP-silica interaction and its effect on hPep-mediated delivery efficiencies. A. Gel electrophoresis of Atto550 tagged gRNA or Cas9 RNP in different buffers. The RNP was unable to migrate through the gel when incubated with PVA-PEG. B. FE-SEM of isolated silica particles from the PVA-EPG solution. Individual particle size appears to range from 20 to 30 nm. Each tick in the scale bar equals 50 nm. C Effect of removal of silica on transfection efficiency of HEK293T SL cells treated with hPep3-RNP. The removal of silica significantly reduced gene editing efficiency (**** < indicating statistical significance of $p < 0.0001$). The data was analyzed using ordinary one way ANOVA multiple comparison between pre-selected pairs and Šídák's multiple comparisons test. Mean value of $n = 3$ independent experiments ± SD. D. Atto550 tagged RNP was formed under different conditions fractioned by centrifugation, with % of Atto550 signal measured in each fraction. Mean value of n = 3 independent experiments ± SD. E. Silica isolated from the PVA-PEG buffer by centrifugation was added to different buffers, with the addition to DMEM/PVA-PEG$_{Pure}$ recapturing the efficiency of RNP-CPP formulated in normal DMEM/PVA-PEG when added to HEK293T SL cells. Note: After dilution into the working buffer, the PVA-PEG contains 0.015% silica. Mean value of n = 3 independent experiments ± SD. F. Envisioned particle formation and structure. Results indicated that the protein adsorbed onto the silica surface, with the peptide interacting with both species. G. Commercial 22 nm Silica beads were added to DMEM and DMEM/PVA-PEG$_{Pure}$ in increasing amounts compared to the PVA-PEG-derived concentration. Adding 1×, 0.015% *w/v*%, the concentration compared to PVA-PEG into PVA-PEG$_{Pure}$ resulted in a similar efficiency as normal PVA-PEG when transfecting HEK293T SL cells. Mean value of n = 3 independent experiments ± SD.

To further explore this effect, Atto550-tagged gRNA was complexed with Cas9 RNP and added to buffers with or without PVA-PEG or hPep3. After centrifugation, Atto550-RNP localized in the pellet fraction in a silica concentration-dependent manner (Fig. 5D). When hPep3 was added, 100% of the Atto550 signal was localized in the pellet, indicating complete encapsulation of the Cas9 RNP. Atto550-labeled complexes were used to further investigate the endocytic uptake of RNP-hPep3 particles. HeLa cells were incubated with the complexes at either 37 °C or 4 °C, yielding a four-fold higher uptake at 37 °C (Supplementary Fig. 5F), consistent with an energy-dependent internalization mechanism. To further explore the involvement of specific endocytic pathways, HeLa cells were treated with various endocytosis inhibitors prior to incubation with RNP-hPep3 (Supplementary Fig. 5G). Although the results were inconclusive, a trend toward reduced uptake was observed upon inhibition of caveolae- and particularly clathrin-mediated endocytosis. This observation aligns with previous findings that CPPs can utilize multiple endocytic routes, and thus, inhibition of a single pathway may not substantially affect overall uptake [61].

Next, the centrifugation-isolated silica was tested by adding it to DMEM, DMEM/PEG8K, and DMEM/PVA-PEG$_{Pure}$ (PVA-PEG without silica) in increasing amounts, along with a fixed amount of RNP:hPep3. Optimal delivery was observed at silica concentrations matching those

found in the PVA-PEG buffer (Fig. 5E & Supplementary Fig. 5H), with PVA-PEG contributing to the effect but to a lesser extent than silica. The envisioned mechanism involves protein adherence to silica, with the CPP binding to silica and RNPs (Fig. 5F).

Commercial 22 nm silica beads were subsequently used with Cas9 RNP in DMEM or DMEM/PVA-PEG$_{Pure}$ to corroborate the silica effect found in PVA-PEG. Maximum editing was achieved when silica concentrations matched those of the PVA-PEG buffer, with results comparable to those of the PVA-PEG containing silica (Fig. 5G).

In conclusion, adding silica is vital for high-efficiency delivery using the hPep system in this configuration. Furthermore, the combination of silica and hPep3 resulted in a 100% encapsulation rate of Cas9 RNP. Lastly, while the silica used in this work was added to the PVA-PEG by the manufacturer, thus potentially reducing reproducibility, our work also shows that it can be replaced by colloidal 22 nm silica.

2.6. Pep3 enables highly efficient and well-tolerated ABE8-mediated base editing of primary human muscle stem cells

In light of the encouraging base editing results achieved in reporter cells and iPSCs, hPep3-mediated base editing was next assessed in therapeutically relevant primary human MuSC. MuSC holds great potential in cell replacement therapies for muscle-wasting disorders, but has been traditionally considered difficult to transfect. The NCAM1 gene encodes for neural cell adhesion molecule 1, a membrane protein ubiquitously expressed in human MuSC [62]. We previously showed that the knock-out of NCAM1 has no negative impact on MuSC fitness ex vivo. Therefore, this gene serves as a universal endogenous reporter locus to assess the efficiency of gene editing interventions in MuSC from any donor. Hence, we targeted a splice donor site in NCAM1 exon 7 using ABE8e (Fig. 6A) [62]. Increasing doses of NCAM1-targeting ABE8e:hPep3 nanoparticles were applied to MuSCs from three donors with a 6-h incubation. This resulted in ~90% A > G conversion at the highest doses 3 days after the treatment, with minimal indel formation (Fig. 6B). Extending the incubation time to 16 h improved editing efficiency, particularly at lower doses (Fig. 6C). The treatment caused a moderate reduction in cell growth during the first three days post-treatment, independent of the editing status. However, the proliferation rate normalized after 3–5 days, remaining comparable to untreated cells throughout the observation period (Fig. 6D and Supplementary Fig. 6A). No significant differences were detected in the expression of key markers such as PAX7 (MuSC marker), Desmin (pan-myogenic marker), or Ki-67 (proliferation marker) between treated and untreated MuSCs at any ABE8:hPep3 dose (Fig. 6E & G, Supplementary Fig. 6B).

Treated MuSCs were induced to fuse into multinucleated myotubes to assess their myogenic potential, mimicking in vivo muscle fibre differentiation. The treated cells retained their ability to form multinucleated myotubes and express the differentiation marker Myosin Heavy Chain (MyHC), showing no adverse effects of the ABE8e treatment (Fig. 6F & H, Supplementary Fig. 6A-D). Lastly, moderate editing efficiencies at lower ABE8e doses were enhanced after a second round of treatment (Supplementary Fig. 7A & B).

These findings demonstrate high editing rates and negligible side effects in these hard-to-transfect cells, suggesting the potential for clinical applications in treating degenerative muscle diseases. This highlights the broad therapeutic implications of the novel CPP formulations developed here.

3. Discussion

Gene editing as a cure for genetic diseases relies on the efficient delivery of relevant effector molecules, such as Cas9-RNPs, which in turn depends upon the level of cargo protection, internalization, and endosomal release. This study optimized the hPep family of cell-penetrating peptides to deliver Cas9 RNP and its derivatives. A key finding in this study is that these peptides can successfully deliver a diverse range of challenging protein cargos, including Cre recombinase and prime editors. Despite its overall cationic charge, Cre recombinase, typically deemed unsuitable for delivery via cationic CPPs, was successfully delivered at editing rates approaching 100%. This underscores the cargo-agnostic potential of this delivery system. Prime editors pose a major challenge due to their considerable size and the highly exposed pegRNA, yet successful, efficient delivery using hPep3 was achieved.

The high editing rates observed in this study can be partially attributed to the introduction of PVA-PEG in the formulation. This additive enhanced editing efficiency by approximately two orders of magnitude compared to the HBG-formulated RNP. During the PVA-PEG production process, silica particles are added to aid the spray-drying process. Silica is known for its ability to adsorb various molecules, including Cas9 RNP, as demonstrated in Fig. 5A. This led us to hypothesize that both the protein and peptide components adhere to the silica surface, with the peptides further interacting with the anionic gRNA (Fig. 5F). Furthermore, the RNP-CPP particles formed in PVA-PEG were smaller than those formed in HBG (Supplementary Fig. 2D). Interestingly, the size of the silica-RNP particles decreased by a third upon the addition of CPPs, indicating a condensation of the RNP absorbed onto the surface of silica. Our hypothesis is reinforced by the successful delivery of Cre, indicating that factors beyond electrostatic interactions between the cargo and the CPP are involved, namely, that of silica adsorption. Using silica as a core for protein and CPP adsorption is crucial as it alters the dynamics and behavior of the resulting nanoparticles. While the application of silica in conjunction with Cas9 RNP is not entirely novel, its combination with CPPs has not been explored previously [56–60]. Incorporating silica to facilitate protein and peptide adsorption could enable previously incompatible cargo and peptide combinations since CPP-mediated non-covalent protein delivery typically relies on the electrostatic interaction between cargo and CPP.

Prime editing, alongside similar techniques like click editing, is heralded as the future of gene editing due to its capacity to make substantial modifications without inducing double-stranded breaks [54]. However, one of the major challenges associated with prime editing is its large size, ≈242 kDa, which is approximately 80 kDa larger than SpCas9, and its highly exposed pegRNA. Consequently, delivering large protein-RNA complexes, such as prime editors in RNP form, poses substantial difficulties, particularly without employing physical methods such as electroporation [63]. Few examples of nanoparticle-based delivery of prime editors exist. One example, conducted by the Mikkelsen lab, utilized lentivirus-derived nanoparticles to achieve around 6% editing in HEK293T cells using PEmax, an optimized variant of PE2 utilized in this study [64]. The second example, published recently by the Lui lab, reported approximately 60% editing using engineered virus-like particles (VLPs) after major engineering the prime editor and pegRNA [65]. Excitingly, hPep3 demonstrated remarkable efficacy, achieving PE2-mediated editing rates approaching 70%. This performance far exceeds the ≈ 20% editing efficiency achieved through nucleofection of PE2 mRNA in the same HEK293T (Fig. 4D). However, it is important to note that different pegRNA targets and specific DNA edits can exhibit varying propensities for successful editing. While the efficiency of prime editing is highly dependent on the guide and local genomic environment, we believe that the hPep delivery system, as such, is largely unaffected by the choice of guide and is thus able to deliver prime editors with different targets equally well.

Additionally, recently published click editors, which operate in a manner similar to prime editing, utilize ssDNA as a template that interacts with a DNA polymerase [66]. While it remains premature to predict which method will dominate the gene-editing landscape in the future, it is apparent that cell-derived nanoparticles, such as VLPs, are unlikely to facilitate the efficient delivery of click editors. This is due to the absence of ssDNA in the cytoplasm, rendering it unavailable for incorporation into gene-editing vectors. Therefore, delivering click editors will likely require a fully synthetic approach akin to the methodology described in this article.

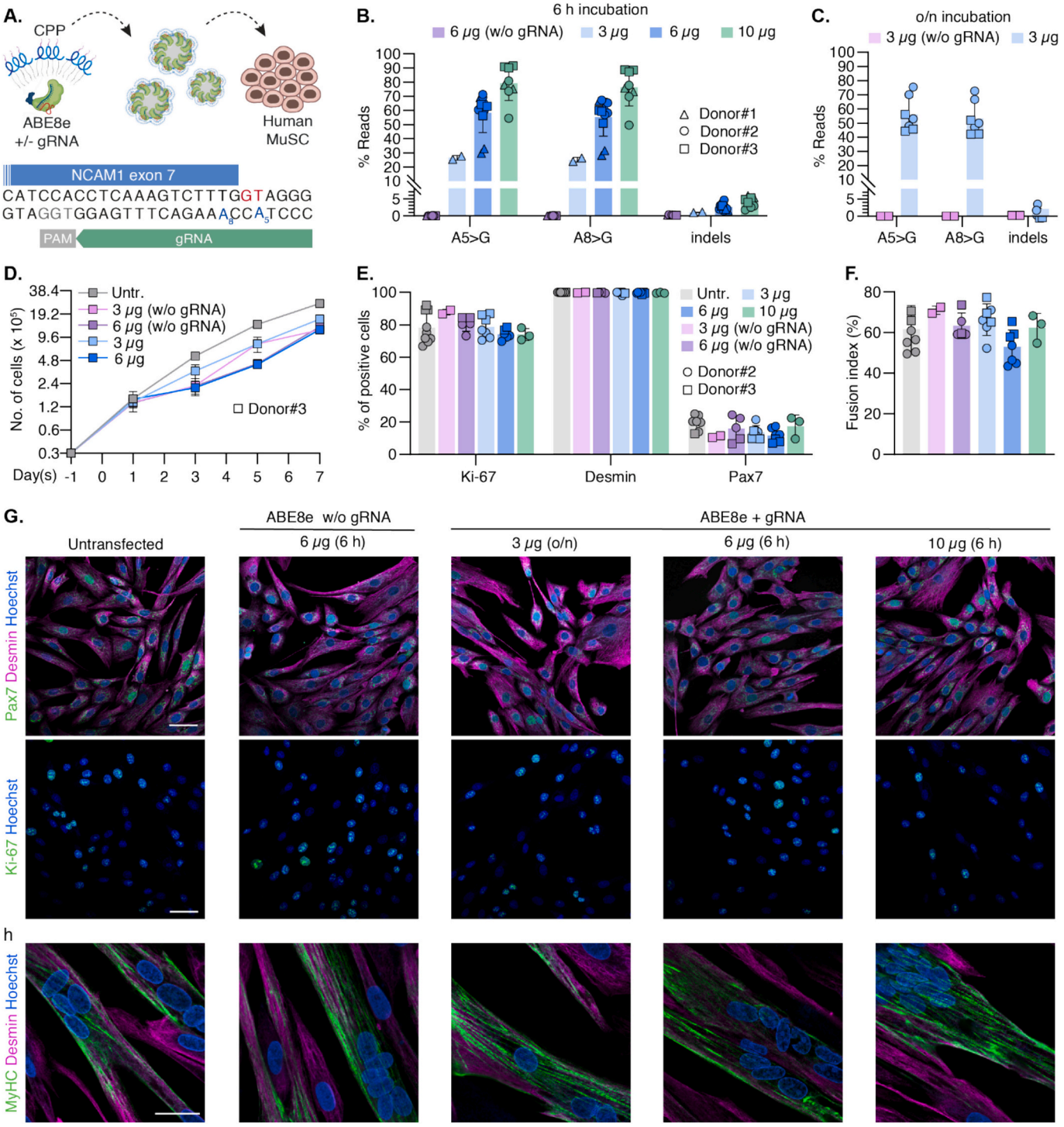

Fig. 6. Editing efficiency, marker expression and morphology of human MuSC. A. Schematic of the experimental set-up. gRNA targeting *NCAM1* exon 7 splice donor site (GT, red). Adenines located at protospacer positions 5 (A_5) and 8 (A_8) are highlighted in blue. The PAM sequence is shown in grey. Cells were grown in 12-well plates, harvested 3 days after treatment followed by processing for gRNA analysis. B. Percentage of NGS reads with A > G conversion at A_5 and A_8 for MuSC from three donors after treatment with hPep3-ABE8e. 3, 6, 10 μg/well corresponds to 12.6, 20.4, 27.2 nM C. Percentage of NGS reads with A > G conversion after treatment with hPep3-ABE8e. D. Growth analysis of human MuSC over 7 days after treatment with hPep3-ABE8e targeting *NCAM1* exon 7 ($n = 2$–3 technical repeats, mean ± SD). Cells were seeded at day −1 and treated at day 0. E. Quantification of myogenic (Pax7, Desmin) and proliferation markers (Ki-67) at day 5 after treatment with hPep3-ABE8e targeting *NCAM1* exon 7 ($n = 2$–6 technical repeats per donor, mean ± SD, ≥ 200 cells/nuclei counted per condition. F. Fusion indices calculated as a percentage of nuclei within multinucleated MyHC-expressing myotubes ($n = 2$–5 technical repeats per donor, mean ± SD, ≥ 200 nuclei were analyzed per condition). G. Confocal microscopy images of MuSC from donor #2 immunostained for myogenic and proliferation markers after treatment with hPep3-ABE8e targeting *NCAM1* exon 7. Scale bars: 50 μm. H. Confocal microscopy images of MuSC from donor #2 induced to fuse into multinucleated myotubes after treatment with hPep3-ABE8e. Scale bar: 50 μm. Untr.: Untransfected. (For interpretation of the references to colour in this figure legend, the reader is referred to the web version of this article.)

While the prime editing presented herein demonstrates noteworthy potential, it is not the only RNP of interest explored in this study. Base editors, such as ABEs and CBEs (cytosine base editors), can correct specific nucleotide substitutions and knock out various genes by disrupting their splice sites. These two widely used base editors can correct approximately 25% of human pathogenic single nucleotide polymorphisms (SNPs), with the ongoing development of new base editors likely to expand this range further [67]. Thus, it is exciting that ABE8e is delivered efficiently, with nearly 100% editing efficiency observed in a reporter target and B2M targeted KO experiments (Fig. 4A & B, Supplementary Fig. 5a). The KO of B2M is relevant for allogenic non-HLA-matched donations of cells to patients, such as in allogenic CAR-T treatments, where the disruption of B2M is one of the proposed initial steps for developing off-the-shelf allogenic CAR-T products [68]. This study also shows the capacity of hPep to deliver Cas9 RNP along with DNA templates, achieving efficient HDR editing in cells with editing levels exceeding 40% without the addition of HDR-enhancing agents (Fig. 2C).

Editing of iPSCs is of great interest because of their ability to differentiate into any cell type. It thus presents tremendous applications to the field for research and therapeutic applications. However, current transfection methods lack efficient delivery and negatively impact cellular viability [69]. Furthermore, no efficient synthetic methods exist for RNP gene editor delivery into iPSCs. In contrast, hPep3-mediated delivery achieves high editing levels (77%) at 6 nM ABE8e while maintaining cellular viability and pluripotency phenotype (Fig. 4C, Supplementary Fig. 5B & C). This is not the first example of nanoparticle RNP delivery to iPSCs. Still, it is an example of unusually efficient nanoparticle RNP delivery and an early example of synthetic nanoparticle base editor delivery to iPSCs [70].

Lastly, the hPep technology shows great potential for delivering gene editors to primary human MuSCs, offering compatibility with downstream applications that demand high editing efficiencies while reducing cytotoxicity. Notably, up to 90% editing was achieved while not adversely affecting the myogenic properties of the cells. The MuSC proliferation rate returned to normal within approximately three days, indicating that MuSCs are well-suited for therapeutic interventions using the hPep system. Comparable high editing efficiencies in human MuSCs have also been reported with mRNA-mediated delivery of ABE and Cas9 via nucleofection [62,71]. However, unlike nucleofection, CPP-mediated delivery is not constrained by cell number requirements, facilitating earlier application and reducing the need for extensive cell passaging and expansion before gene repair. These findings offer promise for developing future MuSC-based gene editing therapies for currently untreatable diseases. A promising direction for such future research would involve repairing mutations in patient-derived MuSCs through hPep3-mediated delivery of various CRISPR enzymes, including prime editors. Additionally, our findings pave the way for novel therapeutic applications in the context of in vivo genome editing of skeletal muscle, an area where progress with non-viral delivery methods for CRISPR tools has been limited [62].

These findings highlight the potential of hPep3 for efficiently delivering diverse protein cargos, applicable across a broad spectrum of cell lines and primary cells. The reagents used are low-cost to produce and straightforward to handle, requiring no specialized equipment. The hPep peptides are comparably priced to commonly used ionizable lipids but do not require the additional helper lipids essential for LNP formulations. Peptide synthesis has become so routine that providers offer fully automated synthesis at kilogram scales. Moreover, the silica component is highly cost-effective; for instance, the 22 nm silica used in Fig. 5G is commercially available in Sweden at approximately $50 per liter (at a ~ 3300× concentration). The synthesis of peptides and silica is well-established and routine, as is the production of proteins and guide RNAs. Consequently, we see no apparent barriers to scaling up or implementing good manufacturing practice production. In its current form, we hope this method will facilitate broader access to gene editing technologies.

4. Materials and methods

4.1. Cell-penetrating peptides

All peptides were procured from Pepscan Presto (Lelystad, The Netherlands) with a purity exceeding 90%. These peptides are terminated with C-terminal amidation and contain a free amine at the N-terminus. All peptides were supplied as lyophilized powder and solubilized in water before use. The sequences of the hPep family of peptides are given in Table 1. The older generation of CPPs tested, TAT (Trans-activating transcriptional), MAP (model amphipathic peptide), TP10 (transportan 10), Penetratin, were labeled with Oregon green 488 to allow for screening of CPP uptake.

4.2. Reagents, chemicals, and media components

The Cas9 protein, CRISPR RNA (crRNA), trans-activating crRNA (trRNA), single-guide RNA (sgRNA), prime editing guide RNA (pegRNA), and oligonucleotides were procured from Integrated DNA Technologies (IDT), Coralville, IA, USA. Guide RNA sequences are available in Table 1. The crRNA, sgRNA, and trRNA contained IDT standard Alt-R™ modifications. The combination of crRNA (or xCRISPR RNA) with trRNA and the sgRNA will henceforth be called gRNA.

Hexametaphosphate, PEG8K, PVP10, PVP50, PVA18, PVA40, PVA-PEG (polyethylene glycol–polyvinyl alcohol, i.e., Kollicoat® IR), HEPES, 22 nm silica (LUDOX® TM-50 colloidal silica), Cell Proliferation Reagent WST-1 (version 18) Roche, and glucose were purchased from Merck, Sweden. The Pure PVA-PEG, an intermediate product in the Kollicoat® IR production, was given as a kind gift from BASF SE (67,056 Ludwigshafen, Germany). Promega Firefly Luciferase Assay System (cat#16174), DAPI (cat# 62248), Lipofectamine™(RNAiMAX) (cat#13778075), Dulbecco's modified Eagle's medium (DMEM®) phenol red free (cat#31053028), DMEM Gluta-Max™ (cat#10564011), Trypsin-EDTA (0.05%), phenol red (cat#25300054) were purchased from Thermo Fisher Scientific (Waltham, MA, USA).

4.3. Protein production

The His-NLS-Cre recombinase (herein called Cre), PCV-Cas9, Adenine base editor 8e (herein called ABE8e), and Prime editor 2 (herein called PE2) (Addgene plasmids: 62730, 123643, 161788, 132775 respectively), were expressed by *Escherichia coli* (BL21 (DE3) T1R pRARE2) upon induction at an optical density of 3 utilizing IPTG. Following induction, the proteins were purified using immobilized metal affinity chromatography using HisTrap HP (GE Healthcare), followed by gel filtration through HiLoad 16/60 Superdex 75 for Cre and Superdex 200 for the Cas9 fusion proteins. The fractions obtained from the gel filtration were assessed via SDS-PAGE gel electrophoresis before combining the main protein fractions. The purified proteins were stored in a storage solution (20 mM HEPES, 300 mM NaCl, 10% glycerol, and 2 mM TCEP, with a pH value of 7.5). We acknowledge Protein Production Sweden for provisioning of facilities and experimental support and we would like to thank Protein Science Facility (PSF) of Karolinska Institutet, Stockholm, Sweden, for assistance. The Swedish Research Council funds Protein Production Sweden as a national research infrastructure. Note that the PE2 (Addgene #132775) was moved into the pNIC-CH2 plasmid, which modified the protein by adding a GS-linker and HIS-tag in the C-terminus. Experiments using ABE8e were performed using protein either from the PSF at KI or provided by Dr. Anja Schütz (Max Delbrück Center Protein Production and Characterization unit).

4.4. Cell lines and cell culture

HeLa, T47D, B16F10, and MSC Traffic light cells were generated in-

house using a lentiviral system with the Addgene plasmid #65726. The HEK293T, MDA-MB-231, and MCF-7 Stoplight cells, used to evaluate Cas9 RNP delivery, were generated as previously described [37,48]. Nozomu Yachie kindly provided the ABE-GFP reporter HEK293T cell line (pLV-CS-121), while the N2A and B16F10 ABE8e reporter cells were generated similarly to the traffic-light cells using the Addgene plasmid #131126 [52]. Unless otherwise stated, Cells were cultured in complete media, DMEM Gluta-Max™ (10% FBS + 1% anti-anti), in a humified incubator at 37 °C with 5% CO_2. Cells were regularly split using trypsin-EDTA (0.05%). Cells were tested for mycoplasma when thawed or frozen.

Karolinska Institutet iPSC Core facility, Stockholm, kindly provided human iPSC lines CTRL-5, CTRL-7, CTRL-9, and CTRL-10. The cells were cultured in mTeSR™ Plus (Stemcell technologies) and seeded as 20,000 cells/cm^2 on 0.5 μg/cm^2 iMatrix511 (Takara Biosciences) in a CO_2 incubator at 37 °C. 5 μM Y-27632 dihydrochloride (Tocris) was added during the first 24 h of the split. Complete media replenishment continues daily with pre-warmed complete mTeSR™ plus media until cells are ready for the next split. Cells were harvested as single cells with 1× TrypLE select (Gibco) during splits and counted using the Countess cell counter (Thermo Fisher Scientific).

Human MuSC isolation was performed as previously described [72]. Immediately after the biopsy procedure, the muscle specimen was transferred into Solution A for transport (30 mM HEPES, 130 mM NaCl, 3 mM KCl, 10 mM D-glucose, and 3.2 μM Phenol red, pH 7.6). The fresh muscle specimen was manually dissected into fragments and then subjected to hypothermic treatment at 5 °C for 4–7 days before downstream processing for MuSC isolation. After hypothermic treatment, fragments were further mechanically dissected, and small fragments were cultured in individual vessels in Skeletal Muscle Cell Growth Medium (SMCGM, Provitro) supplemented with 10% FCS in a humidified incubator with 5% CO_2 at 37 °C to allow outgrowth of oligoclonal MuSC colonies. The outgrowing colonies were expanded and characterized prior to cryopreservation. MuSC populations used in this study are listed in Table 2. For experiments, primary MuSCs were cultured in basal SMCGM enriched with supplement mix (Provitro) in a humidified incubator with 5% CO_2 at 37 °C. For passaging, MuSC were washed with Dulbecco's phosphate-buffered saline (DPBS) (Thermo Fisher Scientific) and detached with 0.25% Trypsin-EDTA (Provitro) or TrypLE Express (Gibco) at 37 °C for 5 min. The medium was switched to Opti-MEM™ I Reduced Serum Media (Thermo Fisher Scientific) once the cells reached confluence to induce fusion into multinucleated myotubes.

4.5. Protein–peptide nanoparticle formation and cell treatment

The protein was added to the buffer tested, followed by the addition of the CPP. This was rapidly followed by vortexing. The protein amount was kept constant at 10 ng/μl, with the CPP being varied according to the final tested molar ratio (MR) between the protein and the CPP. This was done in PCR tubes due to their low binding properties. The complex was allowed to form for 40 min before adding it to the cells. When silica was used, it was directly added into the buffer before adding any protein, at which point the procedure followed. Care was taken not to leave the diluted silica in a buffer not explicitly made for silica storage longer than necessary. For the Cas9 and Cas9 derivatives, the protein was complexed with gRNA at an MR of 1:1.1 protein to RNA. xcrRNA/trRNA was mainly used, but cr/trRNA and sgRNA were also used. No difference in efficiency was seen between the species, so the species were used interchangeably in this study. PegRNA was used for prime editing and treated as a sgRNA for complexation with prime editor 2.

Particles were added to cells, seeded 10 K/well 1 day prior, in complete media (10% FBS with 1% anti-anti) in a 96-well plate unless otherwise stated. The molar ratio used between RNP and CPP was 1:125 unless otherwise noted. The particle-containing media was either left on the cells for the full duration of the experiment or exchanged for fresh media at 2 h (as stated in each figure). Exceptions to this are indicated in the relevant figure. Cells were analyzed between 4 h and 3 days after the addition of the complexes based on the experiment in question (generally 3 days for Cas9 and prime editing treatments and 2 days for ABE8e). HEK293T was used for Cas9, ABE8e, and prime delivery evaluation unless otherwise stated.

The additives were tested by diluting 15 *w/v*% of additive (dissolved in H_2O) in HBG to the desired w/v%. Further testing with PVA-PEG was done by diluting a 10% PVA-PEG (10 w/v% PVA-PEG, 6.3 w/v% sucrose, dissolved in H_2O under heating at 80 °C until dissolved) solution with the desired base solution, often DMEM. The norm for this dilution is 1:1 PVA-PEG 10 w/v% with DMEM forming a 5 w/v% PVA-PEG (3.15 w/v% sucrose) solution.

The iPSCs were treated similarly to the cell lines described above. Briefly, ABE8e:hPep3 particles were added to iPSCs seeded a day prior as 10 K/well in a 96-well flat bottom TC plate in 100 μl. Before particle addition, cells have been given fresh pre-warmed mTESR Plus with 1× Anti/Anti (Gibco). Complete media was replaced 6 h after treatment, followed by another media replacement 1 day after treatment. Cells were stained and analyzed by flow cytometry 3 days after treatment.

For NCAM1 targeting in HEK293T cells, 90 K/well were seeded in 12-well plates 1 day before ABE8e RNP:hPep3 treatment. For PE2 targeting ABE8e reporter cells, 50 K/well HEK293T cells were seeded in a 24-well plate before PE RNP:hPep3 treatment. One day after treatment, the cells were frozen for later analysis. Treated cells were thawed and analyzed by flow cytometry to quantify GFP expression. The media was changed at 4 h after treatment. Cells were harvested for analysis on day 2. For experiments in MuSC, 30 K/well were seeded in 12-well plates 1 day before ABE8e RNP:hPep3 treatment. The media was changed after 6 h or overnight incubation (~16 h), depending on the concentrations added. Cells were harvested for analysis on day 3 after treatment unless otherwise stated.

4.6. RNAiMAX positive control RNP transfection

Transfection using RNAiMAX was conducted according to the protocol optimized by the Chesnut lab [10](10). These transfections were performed in complete media (10% FBS). Unless otherwise stated, editing efficiency was investigated on day 3 after treatment.

4.7. Flow cytometry

Cells were analyzed 4 h to 3 days after treatment to investigate reporter expression. Cells were prepared for the flow cytometry by a PBS wash, followed by trypsin-EDTA (0.05%) digestion. They were stained with DAPI (Thermo Scientific, 25 ng/ml) before analysis by flow cytometry on a MACSQuant Analyzer 10 or 16 (Miltenyi Biotec, Bergisch Gladbach, Germany). Data from this experiment were analyzed using FlowJo 10.6.2 software (FlowJo, LLC).

Antibody staining was done by adding a titrated amount of labeled antibody to single cells, prepared as above, followed by incubation at +4 °C and a wash with PBS to remove any unbound antibody. The live dead stains were performed using DAPI, except for the iPSC, where LIVE/DEAD™ Fixable Aqua Dead Cell stain (L34966, Invitrogen) was used as per manufacturer's instructions after harvesting the cells with TrypLE select. The iPSCs were counterstained with Anti-SSEA4 (1:50, 561565, BD Pharmingen) antibody while staining with B2M (Beta-2 Microglobulin) (1:200, 316312 BioLegend) antibody for 60 min in the dark at +4 °C to identify pluripotency state and B2M KO of the cells

Table 2
MuSC donors used in this study.

Donor ID	Age at biopsy (y)	Gender (m/f)
#1	39	f
#2	25	m
#3	50	m

before acquiring on flow cytometer.

4.8. Storage testing

For vacuum concentration, 50 μl of the prepared complexes were transferred into 1.5 ml microcentrifuge tubes and dried under vacuum conditions using a Thermo Scientific Savant SC210A SpeedVac. The process was conducted without the application of additional heat. The dried samples were resuspended in 50 μl of H_2O before use.

For freeze-drying, the complexes (50 μl) were initially frozen at −80 °C and then transferred into a pre-chilled cooling block maintained at −80 °C. The samples were subjected to vacuum drying until complete desiccation. The lyophilized samples were rehydrated with 50 μl of H_2O before use.

Freeze-thaw cycles were performed by alternately freezing the samples at −80 °C and thawing them at 37 °C.

4.9. WST-1 assay

10 μl of the WST-1 assay reagent (Roche) was added to each well (96-well, 100 μl cell media) and was then incubated between 1 and 2 h. Plates were measured before absorption values went above 2. NT, media only, and lysed cells were used as controls for background and normalization purposes.

4.10. Gal9 imaging experiments and quantitation

Cells were seeded in MatTek glass-bottomed dishes (60,000 cells/35 mm dish) in complete media (DMEM containing 10% FBS) a minimum of 16 h before treatment. Nuclei were uniformly stained with Hoechst 33342 (0.5 μg/ml) added to the culture medium 30 min before imaging experiments. Subsequently, the cell media was replaced with treatment-containing media at selected doses, and the Petri dish was promptly transferred to an inverted Nikon C2+ confocal microscope equipped with a humidified imaging chamber set at 5% CO_2 and 37 °C. Live-cell experiments were conducted using a 60× 1.4 Nikon APO objective and with C2-DUVB GaAsP detectors and variable emission bandpass, employing a 405 nm and 561 nm laser for relevant fluorophores. Images were processed and analyzed using Cell Profiler (v.4.2.6) image-analysis software. Hoechst 33342 facilitated nuclei detection, while diffuse mCherry-GAL9 fluorescence aided in cytoplasm identification. Punctate structures representing ruptured endolysosomes were identified through maximum-intensity projection fluorescence images.

Quantification of spot populations utilized the 'identify primary objects' function within Cell Profiler, discerning punctate structures with intensities surpassing local background cellular intensity and ranging in size from 2 to 35-pixel units. Experimental replicates were averaged from varied individual acquisitions. The resulting data were exported and graphically represented using Origin 2022b.

4.11. Genomic DNA (gDNA) extraction and PCR amplification

Genomic DNA (gDNA) was extracted using Agencourt AMPure XP beads (Beckman Coulter). Briefly, samples were lysed in a heating block at 56 °C for 10 min using AL Buffer (Qiagen) supplemented with Proteinase K (0.2 mg/ml)(Qiagen). Following lysis, double the sample volume of prewarmed AMPure XP beads was added, and the mixture was mixed on a rotational wheel. The tubes were placed on a magnetic rack to separate the bead-bound gDNA from the supernatant. The beads were washed twice with 80% ethanol to remove contaminants, and the bound DNA was eluted with FG3 buffer (Qiagen).

The target region was amplified using Q5 High-Fidelity DNA Polymerase (New England Biolabs). The primer sequences used for amplification are listed in Table 3.

Table 3
Primer sequence for NCAM1ex7 PCR amplification.

Primer	Sequence
NCAM1ex7 (+)	CTGAGGAGTCTTTCCCATTG
NCAM1ex7 (−)	ACTAGGGCTTGGACTAGGTG

4.12. Genome editing analysis by Sanger and next-generation sequencing

PCR products were purified using the NucleoSpin Gel and PCR Clean-up Kit (Macherey-Nagel) according to the manufacturer's protocol. Sanger sequencing was carried out by LGC Genomics (Berlin, Germany), and chromatogram analysis was performed using EditR software (v1.0.10) [73]. For Next-generation amplicon sequencing, samples were analyzed at GENEWIZ (Amplicon EZ service) using an Illumina MiSeq platform and 250 bp paired-end reads. Results were analyzed using CRISPResso2 [74]. The following parameters were applied: Sequencing design: Paired-end reads; Minimum homology for alignment to an amplicon: 60%; Center of the quantification window (relative to the 3′ end of the provided sgRNA): −10; Quantification window size (bp): 10; Minimum average read quality (phred33 scale): >30; Minimum single bp quality (phred33 scale): No filter; Replace bases with N that have a quality lower than (phred33 scale): No filter; Exclude bp from the left side of the amplicon sequence for the quantification of the mutations: 15 bp; Exclude bp from the right side of the amplicon sequence for the quantification of the mutations: 15 bp.

4.13. Gel visualization of RNP-CPP binding (gRNA mobility assay, Hexametaphosphate)

Cas9 and cr/trRNA-Atto550 were complexed 1:1.1 MR, as mentioned above. The RNP was then complexed with CPP in different buffers for 40 min, and a total of 1 pmol RNP was loaded onto a 1% Agarose gel, which ran at 90 V, 200 A for 30 min. The sample was visualized using a Molecular Imager® VersaDoc™ MP 4000 system. Glycerol was added to a final concentration of 5% in samples formulated in any buffer not containing PEG or PVA-PEG to ensure complete loading into the agarose gels. The hexametaphosphate challenge was done by adding increasing amounts of hexametaphosphate for 5 min before loading it onto the gel, as described above.

4.14. Encapsulation

Atto550-RNP was formulated and complexed with CPP, as mentioned earlier. One difference is the use of phenol-red-free DMEM during the experiment. After nanoparticle formation, the complexes were spun at 20000 xg for 30 min. After this, the supernatant was collected, and the pellet was resuspended in the relevant buffer. Both fractions were measured either on the SpectraMax i3x (Molecular Devices, San Jose, CA, USA) or on the CLARIOstar (BMG LABTECH, Ortenberg, Germany) for atto550 content.

4.15. Endocytosis inhibition and uptake studies

Endocytosis inhibitors were added to the cells at the indicated concentrations 30 min prior to treatment with 2 nM Atto550-labeled Cas9 RNP:hPep3 complexes (molar ratio 1:125). Cells were incubated with the RNP:hPep3 complexes and inhibitors for 2 h, followed by a wash with ice-cold PBS. Washed cells were then prepared for flow cytometry and analyzed for Atto550 fluorescence. For the temperature-dependent uptake experiment, cells were pre-incubated at 4 °C for 30 min before the addition of the RNP:hPep3 complexes, and then maintained at 4 °C for 2 h. Flow cytometry analysis was performed as described above.

4.16. Spin-down testing

RNP-CPP particles were formulated as previously described and added to cells in a flat-bottom 96-well spun at 500 *g* or 2000 *g* for 30 min RT. The cells were grown in normal conditions for 3 days before analysis by flow cytometry.

4.17. ZetaView

To determine particle size and concentration of the particles, a PMX-230 ZetaView TWIN instrument (Particle Metrix GmbH, Inning am Ammersee, Germany) was used with the corresponding ZetaView NTA software (8.05.16 SP3) for data analysis. Samples were diluted with HBG buffer before measurement. The following measurement settings were utilized: sensitivity 75, shutter speed 130, and frame rate at 30 frames per second.

4.18. Field emission scanning electron microscope (FE-SEM) and energy-dispersive X-ray spectroscopy (EDS)

The structure and morphology of the freeze-dried samples were analyzed using a field emission scanning electron microscope (FE-SEM; Hitachi S-4800, Japan). The samples were mounted on conductive carbon tape using an accelerated 1–3 kV voltage and a current of 10 μA. The elemental composition of the materials was determined from 3 randomly selected areas for each sample, using the same field emission scanning electron microscope as the electron beam source using an accelerated voltage of 20 kV and a 10 μA current.

4.19. Immunostaining and imaging

Human MuSC were plated on 8-well μ-Slides (ibidis, Germany). For myogenic and proliferation marker staining, 4000 cells/well were seeded and fixed after 2 days. For differentiation, 10,000–12,000 cells were seeded per well as medium was switched to Opti-MEM™ I Reduced Serum Media (Thermo Fisher Scientific) once cells reached 70–80% confluence. Cells were then fixed after 3–5 days with a 4% formaldehyde solution for 10 min at room temperature (RT). Cell permeabilization was performed using 0.2% Triton X-100, and blocking was done with 5% bovine serum albumin (BSA) in DPBS for 1 h at RT. Primary antibodies were incubated overnight at 4 °C in 1% BSA, as indicated in Table 4. Alexa Fluor-conjugated secondary antibodies (Invitrogen) were incubated for 1 h at RT (1:500 in DPBS). Nuclei were counterstained with Hoechst 33342 (Invitrogen). Images were acquired with a laser scanning confocal microscope LSM 900 (Carl Zeiss Microscopy), DMI 6000 fluorescence microscope, and Thunder Imager 3D microscope (Leica Microsystems) and processed with ZEN 3.4 Blue edition (Carl Zeiss Microscopy), Leica Application Suite X (Leica Microsystems), ImageJ (NIH) and Adobe Illustrator 2023. ≥200 nuclei were counted per sample to calculate percentage values for myogenic and proliferation markers. Fusion indices were calculated as the percentage of nuclei within myotubes (defined as ≥2 nuclei in one cell) versus the total number of nuclei captured at 20× magnification. A total of ≥200 nuclei were counted per condition.

4.20. Statistical analysis

All statistical analyses were done using GraphPad Prism (9.2.0), with specific analysis methods described in the relevant figure legend. All error bars are SD, with each experiment being the means of three independent experiments unless otherwise stated.

Table 4
Primary antibodies that are used for immunostaining.

Antibody	Manufacturer (cat#)	Working Dilution
Pax7	Santa Cruz (sc-81648)	1:200
Desmin	Abcam (ab15200)	1:1000
Ki-67	Thermo Fisher Scientific (MA5–14520)	1:300
Skeletal Myosin (fast)	Sigma-Aldrich (M4276)	1:500

CRediT authorship contribution statement

Oskar Gustafsson: Methodology, Project administration, Conceptualization, Writing – original draft, Investigation. **Supriya Krishna:** Visualization, Data curation, Formal analysis, Investigation. **Sophia Borate:** Investigation, Methodology. **Marziyeh Ghaeidamini:** Data curation, Formal analysis, Investigation. **Xiuming Liang:** Investigation. **Osama Saher:** Investigation. **Raul Cuellar:** Visualization, Investigation. **Björn K. Birdsong:** Investigation. **Samantha Roudi:** Investigation, Data curation. **H. Yesid Estupiñán:** Investigation, Visualization. **Evren Alici:** Funding acquisition, Resources. **C.I. Edvard Smith:** Conceptualization. **Elin K. Esbjörner:** Funding acquisition, Resources. **Simone Spuler:** Resources. **Olivier Gerrit de Jong:** Writing – original draft, Methodology, Resources, Supervision. **Helena Escobar:** Resources, Supervision, Conceptualization, Writing – original draft, Investigation. **Joel Z. Nordin:** Writing – original draft, Project administration, Conceptualization, Resources, Funding acquisition, Supervision, Methodology. **Samir E.L. Andaloussi:** Writing – original draft, Methodology, Resources, Conceptualization, Supervision, Funding acquisition.

Funding

European Research Council (ERC) under the European Union's Horizon 2020 research and innovation programme (DELIVER, grant agreement No 101001374) (S.E.A.)

European Union's Horizon 2020 research and innovation programme (EXPERT, grant agreement No 825828) (S.E.A.)

Swedish foundation of Strategic Research FormulaEx, SM19-0007 (S.E.A.)

Cancerfonden project grant 21 1762 Pj 01H (S.E.A.)

Swedish Research Council grant 4–258/2021 (S.E.A.)

Swedish Research Council grant 2021-02407 (J.N.)

CIMED junior investigator grant (J.N.)

Helmholtz Validation fund 2021–2024 (SI.S.)

Declaration of competing interest

Si.S. is an inventor on a technology for primary human muscle stem cell isolation and manufacturing (IP: (DE10 2014 216872), 2015 PCT (WO 2016/030371), granted in EU and US). Si.S. and H.E. are co-inventors on a pending patent application on gene editing of human muscle stem cells (European Patent 666 Office 21 160 696.7). Si.S. is co-founder of MyoPax GmbH and MyoPax Denmark ApS.

Appendix A. Supplementary data

Supplementary data to this article can be found online at https://doi.org/10.1016/j.jconrel.2025.114038.

Data availability

The data that support the findings of this study are available from the corresponding author upon reasonable request.

References

[1] S. Becker, J. Boch, TALE and TALEN genome editing technologies, Gene Genome Ed. 2 (2021) 100007, https://doi.org/10.1016/J.GGEDIT.2021.100007.

[2] F.D. Urnov, E.J. Rebar, M.C. Holmes, H.S. Zhang, P.D. Gregory, Genome editing with engineered zinc finger nucleases, Nat. Rev. Genet. 11 (9) (2010) 636–646, https://doi.org/10.1038/nrg2842.

[3] J.M. Wilson, Lessons Learned from the Gene Therapy Trial for Ornithine Transcarbamylase Deficiency. https://pubmed.ncbi.nlm.nih.gov/19211285/, 2025.

[4] W.L. Chew, M. Tabebordbar, J.K.W. Cheng, P. Mali, E.Y. Wu, A.H.M. Ng, K. Zhu, A. J. Wagers, G.M. Church, A multifunctional AAV-CRISPR-Cas9 and its host response, Nat. Methods 13 (2016) 868–874, https://doi.org/10.1038/NMETH.3993.

[5] R. Mout, M. Ray, Y.W. Lee, F. Scaletti, V.M. Rotello, In vivo delivery of CRISPR/Cas9 for therapeutic gene editing: Progress and challenges, Bioconjug. Chem. 28 (2017) 880–884, https://doi.org/10.1021/ACS.BIOCONJCHEM.7B00057.

[6] K.S. Hanlon, B.P. Kleinstiver, S.P. Garcia, M.P. Zaborowski, A. Volak, S.E. Spirig, A. Muller, A.A. Sousa, S.Q. Tsai, N.E. Bengtsson, C. Lööv, M. Ingelsson, J. S. Chamberlain, D.P. Corey, M.J. Aryee, J.K. Joung, X.O. Breakefield, C.A. Maguire, B. György, High levels of AAV vector integration into CRISPR-induced DNA breaks, Nat. Commun. 10 (1) (2019) 1–11, https://doi.org/10.1038/s41467-019-12449-2.

[7] J.A. Greig, K.M. Martins, C. Breton, R.J. Lamontagne, Y. Zhu, Z. He, J. White, J. X. Zhu, J.A. Chichester, Q. Zheng, Z. Zhang, P. Bell, L. Wang, J.M. Wilson, Integrated vector genomes may contribute to long-term expression in primate liver after AAV administration, Nat. Biotechnol. 42 (8) (2023) 1232–1242, https://doi.org/10.1038/s41587-023-01974-7.

[8] Y. Lin, T.J. Cradick, M.T. Brown, H. Deshmukh, P. Ranjan, N. Sarode, B.M. Wile, P. M. Vertino, F.J. Stewart, G. Bao, CRISPR/Cas9 systems have off-target activity with insertions or deletions between target DNA and guide RNA sequences, Nucleic Acids Res. 42 (2014) 7473–7485, https://doi.org/10.1093/NAR/GKU402.

[9] Y. Fu, J.A. Foden, C. Khayter, M.L. Maeder, D. Reyon, J.K. Joung, J.D. Sander, High-frequency off-target mutagenesis induced by CRISPR-Cas nucleases in human cells, Nat. Biotechnol. 31 (2013) 822–826, https://doi.org/10.1038/NBT.2623.

[10] X. Liang, J. Potter, S. Kumar, Y. Zou, R. Quintanilla, M. Sridharan, J. Carte, W. Chen, N. Roark, S. Ranganathan, N. Ravinder, J.D. Chesnut, Rapid and highly efficient mammalian cell engineering via Cas9 protein transfection, J. Biotechnol. 208 (2015) 44–53, https://doi.org/10.1016/j.jbiotec.2015.04.024.

[11] K. Chen, H. Han, S. Zhao, B. Xu, B. Yin, A. Lawanprasert, M. Trinidad, B. W. Burgstone, N. Murthy, J.A. Doudna, Lung and liver editing by lipid nanoparticle delivery of a stable CRISPR–Cas9 ribonucleoprotein, Nat. Biotechnol. 2024 (2024) 1–13, https://doi.org/10.1038/s41587-024-02437-3.

[12] F.P. Polack, S.J. Thomas, N. Kitchin, J. Absalon, A. Gurtman, S. Lockhart, J. L. Perez, G. Pérez Marc, E.D. Moreira, C. Zerbini, R. Bailey, K.A. Swanson, S. Roychoudhury, K. Koury, P. Li, W.V. Kalina, D. Cooper, R.W. Frenck, L. L. Hammitt, Ö. Türeci, H. Nell, A. Schaefer, S. Ünal, D.B. Tresnan, S. Mather, P. R. Dormitzer, U. Şahin, K.U. Jansen, W.C. Gruber, Safety and efficacy of the BNT162b2 mRNA Covid-19 vaccine, N. Engl. J. Med. 383 (2020) 2603–2615, https://doi.org/10.1056/nejmoa2034577.

[13] E. Sadauskas, H. Wallin, M. Stoltenberg, U. Vogel, P. Doering, A. Larsen, G. Danscher, Kupffer cells are central in the removal of nanoparticles from the organism, Part. Fibre Toxicol. 4 (2007), https://doi.org/10.1186/1743-8977-4-10.

[14] Y. Cao, G.F. Gao, mRNA vaccines: a matter of delivery, EClinicalMedicine 32 (2021), https://doi.org/10.1016/j.eclinm.2021.100746.

[15] S.F. Dowdy, Overcoming cellular barriers for RNA therapeutics, Nat. Biotechnol. 35 (2017) 222–229, https://doi.org/10.1038/nbt.3802.

[16] D.E. Murphy, O.G. de Jong, M.J.W. Evers, M. Nurazizah, R.M. Schiffelers, P. Vader, Natural or synthetic RNA delivery: a stoichiometric comparison of extracellular vesicles and synthetic nanoparticles, Nano Lett. 21 (2021) 1888–1895, https://doi.org/10.1021/acs.nanolett.1c00094.

[17] E.C. Stahl, J.K. Sabo, M.H. Kang, R. Allen, E. Applegate, S.E. Kim, Y. Kwon, A. Seth, N. Lemus, V. Salinas-Rios, K.M. Soczek, M. Trinidad, L.T. Vo, C. Jeans, A. Wozniak, T. Morris, A. Kimberlin, T. Foti, D.F. Savage, J.A. Doudna, Genome editing in the mouse brain with minimally immunogenic Cas9 RNPs, Mol. Ther. 31 (2023) 2422–2438, https://doi.org/10.1016/j.ymthe.2023.06.019.

[18] J.A. Doudna, The promise and challenge of therapeutic genome editing, Nature 578 (2020) 229–236, https://doi.org/10.1038/s41586-020-1978-5.

[19] J. Walther, D. Wilbie, V.S.J. Tissingh, M. Öktem, H. Van Der Veen, B. Lou, E. Mastrobattista, Impact of formulation conditions on lipid nanoparticle characteristics and functional delivery of CRISPR RNP for Gene Knock-out and correction, Pharmaceutics 14 (2022), https://doi.org/10.3390/PHARMACEUTICS14010213/S1.

[20] P.E. Boukany, A. Morss, W.C. Liao, B. Henslee, H. Jung, X. Zhang, B. Yu, X. Wang, Y. Wu, L. Li, K. Gao, X. Hu, X. Zhao, O. Hemminger, W. Lu, G.P. Lafyatis, L.J. Lee, Nanochannel electroporation delivers precise amounts of biomolecules into living cells, Nat. Nanotechnol. 6 (2011) 747–754, https://doi.org/10.1038/NNANO.2011.164.

[21] Y. Chen, S. Aslanoglou, T. Murayama, G. Gervinskas, L.I. Fitzgerald, S. Sriram, J. Tian, A.P.R. Johnston, Y. Morikawa, K. Suu, R. Elnathan, N.H. Voelcker, Silicon-nanotube-mediated intracellular delivery enables ex vivo gene editing, Adv. Mater. 32 (2020), https://doi.org/10.1002/ADMA.202000036.

[22] J. Yen, M. Fiorino, Y. Liu, S. Paula, S. Clarkson, L. Quinn, W.R. Tschantz, H. Klock, N. Guo, C. Russ, V.W.C. Yu, C. Mickanin, S.C. Stevenson, C. Lee, Y. Yang, TRIAMF: a new method for delivery of Cas9 ribonucleoprotein complex to human hematopoietic stem cells, Sci. Rep. 8 (1) (2018) 1–11, https://doi.org/10.1038/s41598-018-34601-6.

[23] Y. Ma, X. Han, O. Quintana Bustamante, R. Bessa De Castro, K. Zhang, P. Zhang, Y. Li, Z. Liu, X. Liu, M. Ferrari, Z. Hu, J. Carlos Segovia, L. Qin, Highly efficient genome editing of human hematopoietic stem cells via a nano-silicon-blade delivery approach, Integr. Biol. (Camb.) 9 (2017) 548, https://doi.org/10.1039/C7IB00060J.

[24] H.X. Wang, M. Li, C.M. Lee, S. Chakraborty, H.W. Kim, G. Bao, K.W. Leong, CRISPR/Cas9-based genome editing for disease modeling and therapy: challenges and opportunities for nonviral delivery, Chem. Rev. 117 (2017) 9874–9906, https://doi.org/10.1021/ACS.CHEMREV.6B00799/ASSET/IMAGES/MEDIUM/CR-2016-00799M_0016.GIF.

[25] J.R. Hamilton, C.A. Tsuchida, D.N. Nguyen, B.R. Shy, E.R. McGarrigle, C. R. Sandoval Espinoza, D. Carr, F. Blaeschke, A. Marson, J.A. Doudna, Targeted delivery of CRISPR-Cas9 and transgenes enables complex immune cell engineering, Cell Rep. 35 (2021), https://doi.org/10.1016/j.celrep.2021.109207.

[26] X. Liang, D. Gupta, J. Xie, E. Van Wonterghem, L. Van Hoecke, J. Hean, Z. Niu, M. Ghaeidamini, O.P.B. Wiklander, W. Zheng, R.J. Wiklander, R. He, D. R. Mamand, J. Bost, G. Zhou, H. Zhou, S. Roudi, H.Y. Estupiñán, J. Rädler, A. M. Zickler, A. Görgens, V.W.Q. Hou, R. Slovak, D.W. Hagey, O.G. de Jong, A.G. Uy, Y. Zong, I. Mäger, C.M. Perez, T.C. Roberts, D. Carter, P. Vader, E.K. Esbjörner, A. de Fougerolles, M.J.A. Wood, R.E. Vandenbroucke, J.Z. Nordin, S. EL Andaloussi, Engineering of extracellular vesicles for efficient intracellular delivery of multimodal therapeutics including genome editors, Nat. Commun. 16 (2025) 4028, https://doi.org/10.1038/s41467-025-59377-y.

[27] S. Ling, X. Zhang, Y. Dai, Z. Jiang, X. Zhou, S. Lu, X. Qian, J. Liu, N. Selfjord, T. M. Satir, A. Lundin, J.L. Touza, M. Firth, N. Van Zuydam, B. Bilican, P. Akcakaya, J. Hong, Y. Cai, Customizable virus-like particles deliver CRISPR–Cas9 ribonucleoprotein for effective ocular neovascular and Huntington's disease gene therapy, Nat. Nanotechnol. (2025), https://doi.org/10.1038/s41565-024-01851-7.

[28] O.P.B. Wiklander, J.Z. Nordin, A. O'Loughlin, Y. Gustafsson, G. Corso, I. Mäger, P. Vader, Y. Lee, H. Sork, Y. Seow, N. Heldring, L. Alvarez-Erviti, C.I. Edvard Smith, K. Le Blanc, P. Macchiarini, P. Jungebluth, M.J.A. Wood, S. El Andaloussi, Extracellular vesicle in vivo biodistribution is determined by cell source, route of administration and targeting, J. Extracell. Ves. 4 (2015) 1–13, https://doi.org/10.3402/jev.v4.26316.

[29] E. Tan, T. Wan, Q. Pan, J. Duan, S. Zhang, R. Wang, P. Gao, J. Lv, H. Wang, D. Li, Y. Ping, Y. Cheng, HEALTH AND MEDICINE Dual-Responsive Nanocarriers for Efficient Cytosolic Protein Delivery and CRISPR-Cas9 Gene Therapy of Inflammatory Skin Disorders. https://www.science.org, 2024.

[30] X. Liu, Z. Zhao, W. Li, Y. Li, Q. Yang, N. Liu, Y. Chen, L. Yin, Engineering nucleotidoproteins for base-pairing-assisted cytosolic delivery and genome editing, Angew. Chem. Int. Ed. 62 (2023), https://doi.org/10.1002/anie.202307664.

[31] S. Ramakrishna, A.B. Kwaku Dad, J. Beloor, R. Gopalappa, S.K. Lee, H. Kim, Gene disruption by cell-penetrating peptide-mediated delivery of Cas9 protein and guide RNA, Genome Res. 24 (2014) 1020, https://doi.org/10.1101/GR.171264.113.

[32] Y. Lin, X. Luo, T. Burghardt, S. Dorrer, M. Höhn, E. Wagner, U. Lächelt, Chemical evolution of amphiphilic Xenopeptides for potentiated Cas9 ribonucleoprotein delivery, J. Am. Chem. Soc. 145 (2023) 15171–15179, https://doi.org/10.1021/JACS.3C01902/ASSET/IMAGES/LARGE/JA3C01902_0006.JPEG.

[33] D.V. Foss, J.J. Muldoon, D.N. Nguyen, D. Carr, S.U. Sahu, J.M. Hunsinger, S. K. Wyman, N. Krishnappa, R. Mendonsa, E.V. Schanzer, B.R. Shy, V.S. Vykunta, V. Allain, Z. Li, A. Marson, J. Eyquem, R.C. Wilson, Peptide-mediated delivery of CRISPR enzymes for the efficient editing of primary human lymphocytes, Nat. Biomed. Eng. 7 (5) (2023) 647–660, https://doi.org/10.1038/s41551-023-01032-2.

[34] B. Suresh, S. Ramakrishna, H. Kim, Cell-penetrating peptide-mediated delivery of Cas9 protein and guide RNA for genome editing, Methods Mol. Biol. 1507 (2017) 81–94, https://doi.org/10.1007/978-1-4939-6518-2_7/FIGURES/7.

[35] K. Chen, E.C. Stahl, M.H. Kang, B. Xu, R. Allen, M. Trinidad, J.A. Doudna, Engineering self-deliverable ribonucleoproteins for genome editing in the brain, Nat. Commun. 15 (1) (2024) 1–11, https://doi.org/10.1038/s41467-024-45998-2.

[36] M. Behr, J. Zhou, B. Xu, H. Zhang, In vivo delivery of CRISPR-Cas9 therapeutics: Progress and challenges, Acta Pharm. Sin. B 11 (2021) 2150–2171, https://doi.org/10.1016/j.apsb.2021.05.020.

[37] M. Öktem, E. Mastrobattista, O.G. de Jong, Amphipathic cell-penetrating peptide-aided delivery of Cas9 RNP for in vitro gene editing and correction, Pharmaceutics 15 (2023) 2500, https://doi.org/10.3390/PHARMACEUTICS15102500/S1.

[38] Z. Zhang, A.E. Baxter, D. Ren, K. Qin, Z. Chen, S.M. Collins, H. Huang, C.A. Komar, P.F. Bailer, J.B. Parker, G.A. Blobel, R.M. Kohli, E.J. Wherry, S.L. Berger, J. Shi, Efficient engineering of human and mouse primary cells using peptide-assisted genome editing, Nat. Biotechnol. 42 (2) (2023) 305–315, https://doi.org/10.1038/s41587-023-01756-1.

[39] J. Mueller, I. Kretzschmar, R. Volkmer, P. Boisguerin, Comparison of cellular uptake using 22 CPPs in 4 different cell lines, Bioconjug. Chem. 19 (2008) 2363–2374, https://doi.org/10.1021/bc800194e.

[40] M. Kosuge, T. Takeuchi, I. Nakase, A.T. Jones, S. Futaki, Cellular internalization and distribution of arginine-rich peptides as a function of extracellular peptide concentration, serum, and plasma membrane associated proteoglycans, Bioconjug. Chem. 19 (2008) 656–664, https://doi.org/10.1021/bc700289w.

[41] J.S. Wadia, R.V. Stan, S.F. Dowdy, Transducible TAT-HA fusogenic peptide enhances escape of TAT-fusion proteins after lipid raft macropinocytosis, Nat. Med. 10 (2004) 310–315, https://doi.org/10.1038/nm996.

[42] N. Bendifallah, F.W. Rasmussen, V. Zachar, P. Ebbesen, P.E. Nielsen, U. Koppelhus, Evaluation of cell-penetrating peptides (CPPs) as vehicles for intracellular delivery of antisense peptide nucleic acid (PNA), Bioconjug. Chem. 17 (2006) 750–758, https://doi.org/10.1021/bc050283q.

[43] J.J. Dowling, C.C. Weihl, M.J. Spencer, Molecular and cellular basis of genetically inherited skeletal muscle disorders, Nat. Rev. Mol. Cell Biol. 22 (11) (2021) 713–732, https://doi.org/10.1038/s41580-021-00389-z.

[44] S. Biressi, A. Filareto, T.A. Rando, Stem cell therapy for muscular dystrophies, J. Clin. Invest. 130 (2020) 5652, https://doi.org/10.1172/JCI142031.

[45] S. Bazaz, T. Lehto, R. Tops, O. Gissberg, D. Gupta, B. Bestas, J. Bost, O.P. B. Wiklander, H. Sork, E.M. Zaghloul, D.R. Mamand, M. Hällbrink, R. Sillard, O. Saher, K. Ezzat, C.I. Edvard Smith, S.E.L. Andaloussi, T. Lehto, Novel

orthogonally hydrocarbon-modified cell-penetrating peptide nanoparticles mediate efficient delivery of splice-switching antisense oligonucleotides in vitro and in vivo, Biomedicines 9 (2021), https://doi.org/10.3390/BIOMEDICINES9081046/S1.
[46] O. Gustafsson, J. Rädler, S. Roudi, T. Lehto, M. Hällbrink, T. Lehto, D. Gupta, S.E. L. Andaloussi, J.Z. Nordin, Efficient peptide-mediated in vitro delivery of Cas9 RNP, Pharmaceutics 13 (2021) 878, https://doi.org/10.3390/PHARMACEUTICS13060878/S1.
[47] A.R. Mól, M.S. Castro, W. Fontes, NetWheels: A web application to create high quality peptide helical wheel and net projections, 2018, https://doi.org/10.1101/416347.
[48] O.G. de Jong, D.E. Murphy, I. Mäger, E. Willms, A. Garcia-Guerra, J.J. Gitz-Francois, J. Lefferts, D. Gupta, S.C. Steenbeek, J. van Rheenen, S. El Andaloussi, R. M. Schiffelers, M.J.A. Wood, P. Vader, A CRISPR-Cas9-based reporter system for single-cell detection of extracellular vesicle-mediated functional transfer of RNA, Nat. Commun. 11 (1) (2020) 1–13, https://doi.org/10.1038/s41467-020-14977-8.
[49] J.A. Zuris, D.B. Thompson, Y. Shu, J.P. Guilinger, J.L. Bessen, J.H. Hu, M. L. Maeder, J.K. Joung, Z.Y. Chen, D.R. Liu, Efficient delivery of genome-editing proteins in vitro and in vivo, Nat. Biotechnol. 33 (2015) 73, https://doi.org/10.1038/NBT.3081.
[50] M.J. Munson, G. O'Driscoll, A.M. Silva, E. Lázaro-Ibáñez, A. Gallud, J.T. Wilson, A. Collén, E.K. Esbjörner, A. Sabirsh, A high-throughput Galectin-9 imaging assay for quantifying nanoparticle uptake, endosomal escape and functional RNA delivery, Commun. Biol. 4 (2021), https://doi.org/10.1038/S42003-021-01728-8.
[51] M.F. Richter, K.T. Zhao, E. Eton, A. Lapinaite, G.A. Newby, B.W. Thuronyi, C. Wilson, L.W. Koblan, J. Zeng, D.E. Bauer, J.A. Doudna, D.R. Liu, Phage-assisted evolution of an adenine base editor with improved Cas domain compatibility and activity, Nat. Biotechnol. 38 (2020) 883, https://doi.org/10.1038/S41587-020-0453-Z.
[52] R.C. Sakata, S. Ishiguro, H. Mori, M. Tanaka, K. Tatsuno, H. Ueda, S. Yamamoto, M. Seki, N. Masuyama, K. Nishida, H. Nishimasu, K. Arakawa, A. Kondo, O. Nureki, M. Tomita, H. Aburatani, N. Yachie, Base editors for simultaneous introduction of C-to-T and A-to-G mutations, Nat. Biotechnol. 38 (7) (2020) 865–869, https://doi.org/10.1038/s41587-020-0509-0.
[53] M.G. Kluesner, W.S. Lahr, C. Lonetree, B.A. Smeester, X. Qiu, N.J. Slipek, P.N. Claudio Vázquez, S.P. Pitzen, E.J. Pomeroy, M.J. Vignes, S.C. Lee, S.P. Bingea, A. A. Andrew, B.R. Webber, B.S. Moriarity, CRISPR-Cas9 cytidine and adenosine base editing of splice-sites mediates highly-efficient disruption of proteins in primary and immortalized cells, Nat. Commun. 12 (2021) 1–12, https://doi.org/10.1038/s41467-021-22009-2.
[54] A.V. Anzalone, P.B. Randolph, J.R. Davis, A.A. Sousa, L.W. Koblan, J.M. Levy, P. J. Chen, C. Wilson, G.A. Newby, A. Raguram, D.R. Liu, Search-and-replace genome editing without double-strand breaks or donor DNA, Nature 576 (2019) 149–157, https://doi.org/10.1038/s41586-019-1711-4.
[55] J. Meissner, A. Prause, B. Bharti, G.H. Findenegg, Characterization of protein adsorption onto silica nanoparticles: influence of pH and ionic strength, Colloid Polym. Sci. 293 (2015) 3381, https://doi.org/10.1007/S00396-015-3754-X.
[56] A.E. LaBauve, E.A. Saada, I.K.A. Jones, R. Mosesso, A. Noureddine, J. Techel, A. Gomez, N. Collette, M.B. Sherman, R.E. Serda, K.S. Butler, C.J. Brinker, J. S. Schoeniger, D. Sasaki, O.A. Negrete, Lipid-coated mesoporous silica nanoparticles for anti-viral applications via delivery of CRISPR-Cas9 ribonucleoproteins, Sci. Rep. 13 (1) (2023) 1–13, https://doi.org/10.1038/s41598-023-33092-4.
[57] Y. Wang, P.K. Shahi, X. Wang, R. Xie, Y. Zhao, M. Wu, S. Roge, B.R. Pattnaik, S. Gong, In vivo targeted delivery of nucleic acids and CRISPR genome editors enabled by GSH-responsive silica nanoparticles, J. Control. Release 336 (2021) 296–309, https://doi.org/10.1016/J.JCONREL.2021.06.030.
[58] P.R. Salekdeh, L. Ma'mani, J. Tavakkoly-Bazzaz, H. Mousavi, M.H. Modarressi, G. H. Salekdeh, Bi-functionalized aminoguanidine-PEGylated periodic mesoporous organosilica nanoparticles: a promising nanocarrier for delivery of Cas9-sgRNA ribonucleoproteine, J. Nanobiotechnol. 19 (2021) 1–16, https://doi.org/10.1186/S12951-021-00838-Z/METRICS.
[59] A. Noureddine, A. Maestas-Olguin, E.A. Saada, A.E. LaBauve, J.O. Agola, K.E. Baty, T. Howard, J.K. Sabo, C.R.S. Espinoza, J.A. Doudna, J.S. Schoeniger, K.S. Butler, O. A. Negrete, C.J. Brinker, R.E. Serda, Engineering of monosized lipid-coated mesoporous silica nanoparticles for CRISPR delivery, Acta Biomater. 114 (2020) 358–368, https://doi.org/10.1016/J.ACTBIO.2020.07.027.
[60] Y. Wang, X. Wang, R. Xie, J.C. Burger, Y. Tong, S. Gong, Overcoming the blood–brain barrier for gene therapy via systemic administration of GSH-responsive silica nanocapsules, Adv. Mater. 35 (2023), https://doi.org/10.1002/adma.202208018.
[61] J.C. LeCher, S.J. Nowak, J.L. McMurry, Breaking in and busting out: cell-penetrating peptides and the endosomal escape problem, Biomol. Concepts 8 (2017) 131–141, https://doi.org/10.1515/bmc-2017-0023.
[62] C. Stadelmann, S. Di Francescantonio, A. Marg, S. Müthel, S. Spuler, H. Escobar, mRNA-mediated delivery of gene editing tools to human primary muscle stem cells, Mol. Ther. Nucl. Acids 28 (2022) 47–57, https://doi.org/10.1016/J.OMTN.2022.02.016.
[63] K. Petri, W. Zhang, J. Ma, A. Schmidts, H. Lee, J.E. Horng, D.Y. Kim, I.C. Kurt, K. Clement, J.Y. Hsu, L. Pinello, M.V. Maus, J.K. Joung, J.R.J. Yeh, CRISPR prime editing with ribonucleoprotein complexes in zebrafish and primary human cells, Nat. Biotechnol. 40 (2022) 189, https://doi.org/10.1038/S41587-021-00901-Y.
[64] J. Haldrup, S. Andersen, A.R. LaVilla Labial, J.H. Wolff, F.P. Frandsen, T.W. Skov, A.B. Rovsing, I. Nielsen, T.S. Jakobsen, A.L. Askou, M.K. Thomsen, T.J. Corydon, E. A. Thomsen, J.G. Mikkelsen, Engineered lentivirus-derived nanoparticles (LVNPs) for delivery of CRISPR/Cas ribonucleoprotein complexes supporting base editing, prime editing and in vivo gene modification, Nucleic Acids Res. 51 (2023) 10059–10074, https://doi.org/10.1093/NAR/GKAD676.
[65] M. An, A. Raguram, S.W. Du, S. Banskota, J.R. Davis, G.A. Newby, P.Z. Chen, K. Palczewski, D.R. Liu, Engineered virus-like particles for transient delivery of prime editor ribonucleoprotein complexes in vivo, Nat. Biotechnol. 2024 (2024) 1–12, https://doi.org/10.1038/s41587-023-02078-y.
[66] J. Ferreira da Silva, C.J. Tou, E.M. King, M.L. Eller, D. Rufino-Ramos, L. Ma, C. R. Cromwell, J. Metovic, F.M.C. Benning, L.H. Chao, F.S. Eichler, B.P. Kleinstiver, Click editing enables programmable genome writing using DNA polymerases and HUH endonucleases, Nat. Biotechnol. 2024 (2024) 1–13, https://doi.org/10.1038/s41587-024-02324-x.
[67] H.A. Rees, D.R. Liu, Base editing: precision chemistry on the genome and transcriptome of living cells, Nat. Rev. Genet. 19 (2018) 770, https://doi.org/10.1038/S41576-018-0059-1.
[68] J. Ren, X. Liu, C. Fang, S. Jiang, C.H. June, Y. Zhao, Multiplex genome editing to generate universal CAR T cells resistant to PD1 inhibition, Clin. Cancer Res. 23 (2017) 2255, https://doi.org/10.1158/1078-0432.CCR-16-1300.
[69] S. Tan, Z. Tao, S. Loo, L. Su, X. Chen, L. Ye, Non-viral vector based gene transfection with human induced pluripotent stem cells derived cardiomyocytes, Sci. Rep. 9 (1) (2019) 1–11, https://doi.org/10.1038/s41598-019-50980-w.
[70] K. Lee, M. Conboy, H.M. Park, F. Jiang, H.J. Kim, M.A. Dewitt, V.A. Mackley, K. Chang, A. Rao, C. Skinner, T. Shobha, M. Mehdipour, H. Liu, W.C. Huang, F. Lan, N.L. Bray, S. Li, J.E. Corn, K. Kataoka, J.A. Doudna, I. Conboy, N. Murthy, Nanoparticle delivery of Cas9 ribonucleoprotein and donor DNA in vivo induces homology-directed DNA repair, Nat. Biomed. Eng. 1 (2017) 889, https://doi.org/10.1038/S41551-017-0137-2.
[71] S. Müthel, A. Marg, B. Ignak, J. Kieshauer, H. Escobar, C. Stadelmann, S. Spuler, Cas9-induced single cut enables highly efficient and template-free repair of a muscular dystrophy causing founder mutation, Mol. Ther. Nucl. Acids 31 (2023) 494–511, https://doi.org/10.1016/J.OMTN.2023.02.005.
[72] A. Marg, H. Escobar, N. Karaiskos, S.A. Grunwald, E. Metzler, J. Kieshauer, S. Sauer, D. Pasemann, E. Malfatti, D. Mompoint, S. Quijano-Roy, A. Boltengagen, J. Schneider, M. Schülke, S. Kunz, R. Carlier, C. Birchmeier, H. Amthor, A. Spuler, C. Kocks, N. Rajewsky, S. Spuler, Human muscle-derived CLEC14A-positive cells regenerate muscle independent of PAX7, Nat. Commun. 10 (1) (2019) 1–11, https://doi.org/10.1038/s41467-019-13650-z.
[73] M.G. Kluesner, D.A. Nedveck, W.S. Lahr, J.R. Garbe, J.E. Abrahante, B.R. Webber, B.S. Moriarity, EditR: a method to quantify Base editing from Sanger sequencing, CRISPR J. 1 (2018) 239, https://doi.org/10.1089/CRISPR.2018.0014.
[74] K. Clement, H. Rees, M.C. Canver, J.M. Gehrke, R. Farouni, J.Y. Hsu, M.A. Cole, D. R. Liu, J.K. Joung, D.E. Bauer, L. Pinello, CRISPResso2 provides accurate and rapid genome editing sequence analysis, Nat. Biotechnol. 37 (3) (2019) 224–226, https://doi.org/10.1038/s41587-019-0032-3.